e-Prime - Advances in Electrical Engineering, Electronics and Energy 2 (2022) 100027

Contents lists available at ScienceDirect

e-Prime - Advances in Electrical Engineering, Electronics and Energy

journal homepage: www.elsevier.com/locate/prime

Flexible nuclear plants with thermal energy storage and secondary power cycles: Virtual power plant integration in a UK energy system case study

Panagiotis Romanos[a], Abdullah A. Al Kindi[b], Antonio M. Pantaleo[b], Christos N. Markides[b,*]

[a] Romanos Engineering Consultancy Ltd., Sheffield, UK
[b] Clean Energy Processes (CEP) Laboratory, Department of Chemical Engineering, Imperial College London, London, UK

ARTICLE INFO

Keywords:
Flexible energy system
Nuclear power
Organic Rankine cycle
Phase change materials
Thermal energy storage
Virtual power plant

ABSTRACT

Electricity markets are fast changing because of the increasing penetration of intermittent renewable generation, leading to a growing need for the flexible operation of power plants to provide regulation services to the grid. Previous studies have suggested that conventional power plants (e.g., nuclear) may benefit from the integration of thermal energy storage (TES), as this enables greater flexibility. In conventional Rankine-cycle power plants, steam can be extracted during off-peak periods to charge TES tanks filled with phase-change materials (PCMs); at a later time, when this is required and/or economically favourable, these tanks can feed secondary thermal power plants to generate power, for example, by acting as evaporators of organic Rankine cycle (ORC) plants. This solution offers greater flexibility than TES-only solutions that store thermal energy and then release this back to the base power plant, as it allows both derating and over-generation. The solution is applied here to a specific case study of a 670 MW_{el} nuclear power plant in the UK, which is a typical baseload power plant not intended for flexible operation. It is found a maximum combined power of 822 MW_{el} can be delivered during peak demand, which is 23% higher than the base plant's (nominal) rated power, and a maximum derating of 40%, i.e., down to 406 MW_{el} during off-peak demand. An operational energy management strategy (EMS) is then proposed for optimising the charging of the TES tanks during off-peak demand periods and for controlling the discharging of the tanks for electricity generation during peak-demand periods. An economic analysis is performed to evaluate the potential benefits of this EMS. Profitability in the case study considered here can result when the average peak and off-peak electricity price variations are at least double those that occurred in the UK market in 2019 (with recent data now close to this), and when TES charge/discharge cycles are performed more than once per day with a discharge duration to the ORC plants longer than 2 h. When considering the most recent UK electricity prices in 2021 (to-date), the EMS investment cost for one 1-h charge and 1-h discharge cycle per day is 199 m£ with a total generation of 50 GWh per year and a levelised cost of electricity (LCOE) of 463 £/MWh. The investment cost drops significantly to 48 m£ when discharging for a longer duration of 8 h as the size of the ORC plants decrease. The projected LCOE also decreases to 159 £/MWh when doubling the total generated electricity (100 GWh/year) by employing two 8-h TES charge/discharge cycles per day. Importantly, it is found that the economics of the EMS are determined by a trade-off between longer discharge durations to the ORC plants that minimises their size and cost, and shorter charge/discharge durations that yield the highest spread between off-peak and peak electricity prices.

1. Introduction

Advanced operating procedures to optimise reserve capacity and flexibility of conventional generation can be introduced to manage the intermittency in power grids associated with the penetration of variable renewable energy sources (VRES) [1]. The growth of VRES has a significant impact on the operation of traditional electricity generation fleets, and many efficient units built for baseload operation are today being used inefficiently, since the despatch priority is given to VRES. As solar irradiance and wind speed vary, conventional generation units are required to ramp up and down, in many cases even beyond their flexibility limits. VRES unpredictability forces transmission system operators (TSO) to increase spinning reserve capacity, ready to provide additional power when VRES generation produces less power than the forecast and vice versa. The growth of VRES also influences electricity markets in many countries, producing unexpected wholesale price reduction, new merit order related to VRES dispatching priority, changes in ancillary services and balancing costs. Flexibility is needed for generation to re-

* Corresponding author.
E-mail address: c.markides@imperial.ac.uk (C.N. Markides).

https://doi.org/10.1016/j.prime.2021.100027
Received 4 September 2021; Received in revised form 4 December 2021; Accepted 14 December 2021

Nomenclature*

Symbols

A	area (m^2)
C	capital cost (£)
CH	charging cost (£)
c_p	specific heat capacity (J/kg·K)
CP	capacity payment (£)
d	diameter (m)
D	tank diameter (m)
E	electricity (Wh, J)
EP	electricity price (£/Wh)
f	waviness correction factor (-)
F	flow parameter (-)
g	acceleration of gravity (m/s^2)
h	specific enthalpy (J/kg)
H	enthalpy (J)
$\dot{H}$	rate of enthalpy (W)
I	annual income (£)
k	thermal conductivity (W/m·K)
K	correction factor (-)
L	length (m)
$LCOE$	levelised cost of electricity (£/Wh)
m	mass (kg)
$\dot{m}$	mass flowrate (kg/s)
n	lifetime (years)
NPV	net present value (£)
Nu	Nusselt number (-)
$O\&M$	operation and maintenance cost (£)
P	pressure (bar, Pa)
Pr	Prandtl number (-)
Q	heat (J)
q'	heat flux (W/m^2)
$\dot{Q}$	rate of heat (W)
r	discount rate (%)
Re	Reynolds number (-)
s	specific entropy (J/kg·K)
S	entropy (J/K)
$\dot{S}$	rate of entropy (W/K)
t	time (s)
T	temperature (°C, K)
u	velocity (m/s)
U	overall heat transfer coefficient (W/m^2·K)
v	kinematic viscosity (m^2/s)
V	volume (m^3)
w	tube thickness (m)
$\dot{W}$	power (W)
x	quality (-)
$\dot{x}$	local dryness factor (-)
z	distance (m)

Greek symbols

α	heat transfer coefficient (W/m^2·K)
δ	thickness (m)
Δ	change between two values (-)
ε	volumetric vapour-phase fraction (-)
η	efficiency (-)
θ	temperature (°C, K)
Λ	Nusselt film height (m)
μ	dynamic viscosity (kg/m·s)
ξ	friction factor (-)
ρ	density (kg/m^3)
τ	shear stress (N/m^2)

Subscripts/superscripts

a	ambient
Ch	charging
cond	condensing
CP	condensate pump
crit	critical
d	dead-state
Dch	discharging
evap	evaporation
EMS	energy management system
F	film
FP	feed pump
g	smooth
G	generator
i	inner
IHX	internal heat exchanger
in	inlet
is	isentropic
L	liquid
La	laminar
LM	logarithmic mean
m	melting
max	maximum
min	minimum
net	net
o	outer
ORC	organic Rankine cycle
out	outlet
P	pump
PCM	phase change material
Ph	film free-surface
pp	pinch point
r	rough
s	surface
sat	saturation
SE	side extraction
T	turbine
TES	thermal energy storage
TT	thermal tank
TT-1	Thermal Tank 1
TT-2	Thermal Tank 2
TT-3	Thermal Tank 3
Tu	turbulent
Ü	superheated
v	vaporisation
V	vapour
w	wall

Acronyms

AGR	advanced gas-cooled reactor
AOP	average off-peak price
BM	balancing market
CCGT	combined cycle gas turbine
CSP	concentrated solar power
EdF	Electricite de France
EMS	energy management system
FFR	fast frequency response
HPT	high-pressure turbine
IPT	intermediate-pressure turbine
LCOE	levelised cost of electricity
LWR	light water reactor

LPT	low-pressure turbine
NIV	net imbalance volume
NPV	net present value
ORC	organic Rankine cycle
PCM	phase change material
PD	price difference
TES	thermal energy storage
TSO	transmission system operator
VRES	variable renewable energy sources
VPP	virtual power plant

spond rapidly to the changing load conditions that has required short start-up and shut-down times compared to steady base-load operation. The need for fast ramp up and down mode imposes additional costs, including increased maintenance cost wear, lower efficiency at part load and increased overall emissions.

It is recognised that the energy market alone does not provide price signals which are sufficiently strong and effective for long-term planning and security of supply in case of high VRES penetration. Effective market redesign practices include capacity payments, where generators are remunerated for being available to provide spinning reserve to the grid, or faster scheduling of the electricity market, with hourly and sub-hourly scheduling, that allows a more efficient use of available transmission/generation capacity, lower reserve requirements thanks to a shorter and more accurate forecast of VRES, and negative market price, which are signals on the wholesale power market when highly inflexible power generation meets low demand and high VRES generation.

In order to minimise the impact on the grid of high share of VRES, in some countries the intermittent generators are required to aggregate into a virtual power plant (VPP). A VPP is a cluster of dispersed generator units, controllable loads and storages systems, which can operate as a unique power plant, through an energy management system (EMS) which coordinates the power flows coming from the generators, controllable loads and storages [2,3]. Such asset of generation and storage technologies could include flexible generation systems, able to compensate the intermittency of VRES.

Moreover, the connection of asynchronous generators to electricity transmission networks due to the high penetration of renewables can result in grid frequency variations, which could exceed given thresholds [4], so that the per unit drop or speed regulation of synchronous generator units can no longer respond adequately, and this can ultimately lead to brownouts or even blackouts. Appropriate energy management actions are thus required in response to such frequency variations, such as curtailment, demand-side management or fast response of conventional generation systems.

Curtailment results in wasted energy from renewable sources while energy is taken instead from mainly fossil-fuelled power plants, leading to a direct reduction of capacity factors of renewable energy generation. On the other hand, smart electricity grids provide a solution based on the development of an appropriate topology for integrating electrical energy transmission, distribution and storage technologies and systems. Battery banks can provide ancillary services for primary and secondary frequency control thanks to their very fast response [5]. However, this is a relatively expensive solution and there are issues that emerge from its embodied materials, energy and emissions, especially for large-scale applications in bulk power systems.

In this paper, we consider a flexible generation-integrated EMS featuring the integration of thermal energy storage (TES) based on phase-change materials (PCMs) and organic Rankine cycle (ORC) units into a nuclear power plant. The proposed solution can be applied with few modifications to other types of Rankine-cycle (e.g., coal-fired) power plants, or gas-turbine and combined power plants. The latter are of interest since they are characterised by flexible unit despatch and load-following operations [6], while also having the highest electric efficiencies of all thermal power plants, often exceeding 60% [7] (in fact, the efficiency of such plants can reach values up to 65% when improving gas-turbine technology and optimising the heat recovery steam generator [8]).

During off-peak demand, steam can be extracted from such power plants for the charging of an array of PCM based thermal tanks. At a later time, when this is required and/or economically favourable, the charged TES tanks can discharge heat to secondary ORC power plants in order to generate power in addition to that of the base power plant. ORC plants are of particular relevance in this context as they are suitable for power generation at reduced temperatures and smaller scales [9–12]. The study of this type of solution is of interest as it offers greater flexibility than TES-only solutions that store thermal energy and then release this back to the base power plant, by allowing over-generation during peak demand whereby the total available power output is higher than the base plant's rated capacity, thanks to the additional power delivered by the secondary power plants. In such an EMS scheme, it is of interest to optimise the derating of the power plants for the charging of the thermal tanks and to control the discharging of the tanks for electricity generation from the secondary plants.

The use of TES technology based on PCMs is nowadays common practice in some large-scale power generation applications. Such TES, without secondary power generation as is mentioned above, is for example regularly integrated in concentrated solar power (CSP) plants in order to support this intermittent energy source and also to allow load-following operations [13]. In fact, the integration of TES in CSP can increase the solar share (fraction of total energy provided by solar) by as much as 47%, to over 70% on sunny days [14]. Furthermore, the round-trip efficiencies of TES units comprising two tanks with hot (high-temperature) and cold (low-temperature) salts are above 97% [15], lending an important competitive advantage to CSP technology (e.g., relative to photovoltaics) given the lower cost of thermal versus electrical energy storage for improved dispatchability and load-following operations [16]. The challenge concerning the development and practical integration of TES systems into conventional power plants (nuclear, coal, etc.) can be strongly facilitated by harnessing the CSP experience.

Coal-fired power plants often represent a large share of the power delivered to grids, and could be operated to improve grid stability with great effectiveness in the scenario of a significant generation of intermittent renewable electricity. An interesting option, for example, involves the conversion of heat to electricity at peak-demand times by integrating waste heat in the feedwater preheating systems of such plants, as investigated by Roth et al. [17] in a 390 MW_{el} coal-fired power plant. Grid stability can be further enhanced by means of secondary frequency-control strategies. For example, Zehtner et al. [18] evaluated the response of the 450 MW_{el} hard-coal power plant in Germany, when different condensate throttling and feedwater oversteering variants were applied aimed at secondary frequency control. Of particular interest, as this can significantly enhance grid flexibility, is the reliable operation of such power plants during negative load changes, such as in the study of Starkloff et al. [19] that considered a load change from 100% to 28% in a large once-through coal-fired power plant in Germany. Finally, TES integration into coal-fired power plants has been proposed to enhance flexibility and load-following operations [20].

Unlike coal-fired plants that can be modulated to some extent according to the demand, nuclear power plants are more suitable for delivering "baseload" electrical power in what is not conventionally considered flexible generation. Yet, even in this case, flexibility is highly desirable, and efforts have been underway to increase generation flexibility. Modern Generation III (and its evolution, Gen. III+) nuclear reactors are capable of a certain degree of flexibility and load-following operations, with transmission system operators (TSOs) able to define the minimum

* N.B.: Other symbols are defined in the text where they are first used. Where appropriate, lower-case symbols refer to specific quantities and upper-case symbols to extensive quantities.

requirements of such reactors [21–23]. The European utility standards require that nuclear power plants are capable of (at least) daily load-cycling operation between 50% and 100% of their nominal capacity, with a rate of change of generation output of 3–5% of nominal capacity per minute [22]. Although the solution proposed here can be used to exceed the minimum (50%) load requirement in Gen. III+ power plants, thereby allowing flexibility beyond the aforementioned capabilities, the present study focuses on flexible operations and load-following capabilities by retrofitting the solution to existing (Gen. I and II) nuclear power plants, since the flexibility of these nuclear power plants may be considered a more pressing issue in present power systems.

Persson et al. [24] conducted a comprehensive review of the experience with load-following in France, Germany, Sweden and the USA, as well as of the technical aspects of output changes in nuclear power plants, focusing on the capability of nuclear power plants to complement the fluctuating power supply from renewables in Sweden. A similar study was conducted for nuclear power plants in Germany by Ludwig et al. [25]. Both studies investigate the possibilities of using nuclear power plants, either in Sweden or Germany, for flexible load-following power generation with minimum loads down to 50–65%, concluding that improved flexibility (ranges and rates) are possible with suitable changes such as optimised fuel management, optimised control of manoeuvring and predictive operating strategies [24,25]. Moreover, Al Kindi et al. [26] examines the flexibility and the cycle efficiency of a hybrid nuclear-solar power plant integrated with TES (molten salt) system. The study concluded that flexibility could be achieved between 55% and 100% through indirect TES integration and while operating the small modular nuclear reactor unit at full load. It is therefore expected that the flexible operation of nuclear power plants can be considerably increased with the integration of TES systems, as is considered here.

The coupling of nuclear reactors with TES systems for the purpose of improving flexibility and increasing revenues has been proposed and studied previously [27–40]. For example, Carlson et al. [27] studied the impact of integrating a TES tank within a primary power generation Rankine cycle in a modern nuclear reactor. Two flexibility options were studied: (i) bypassing steam from the steam generator and sending this directly to the condenser; and (ii) storing heat from the excess steam in TES tanks, and then discharging this into the primary cycle during periods of peak demand. The second option showed a potential for increasing the capacity factor of the nuclear power plant by almost 10% compared to the steam bypass option. The capacity factor could be further increased if more TES charging/discharging cycles are performed. Carlson et al. [28] also investigated, using thermodynamic cycle analysis, three alterative configurations of nuclear plants integrated with TES tanks and secondary power-cycle systems. These configurations are distinguished by the location of steam extraction from the primary power cycle, and all use a secondary power generation system that is connected to the attached TES tanks. It was found that the configuration where the TES tanks are charged with heat from steam diverted after the moisture separator/reheater had the greatest thermodynamic benefits. Furthermore, this configuration provided greater flexibility, with a 15% increase in the capacity factor compared to the steam bypass option (i.e., the first option).

Carlson et al. [29] extended their research by performing a thermo-economic analysis of coupling a pressurised water reactor (Westinghouse AP1000) with a TES system and a secondary Rankine cycle. The study proposed and investigated three different configurations that are distinguished by charging/discharging mechanisms and durations of the TES tanks. The results showed that the addition of a secondary generator could provide more than 1.5 times the nominal power output of 1050 MW_{el}. From an economic perspective, the study recommended the use of a rock bed (i.e., sensible heat storage) rather than latent heat storage materials due to the high cost of eutectic salt mixtures.

There are several studies that discuss the increased flexibility and the potential economic benefits of adding TES systems to nuclear power plant. For example, Denholm et al. [30] explored the benefits of adding flexibility on nuclear reactors by combining it with a two-tank molten-salt based TES system and a power generation block that is sized at 150% of the reactor output. It was concluded that adding a TES system could result in increased capacity factors and potentially lower levelised cost of electricity (LCOE) when operating nuclear power plants in electricity grids that have a high penetration of renewables. Moreover, Forsberg [31] studied the potential profitability of integrating light water reactors (LWRs) with a heat storage system and a combustion heat source. Forsberg [31] concluded that the economics of such integration depends on three factors: (i) the price of the heat storage system is less than electricity storage technologies (e.g., batteries); (ii) the cost of the nuclear steam supply system is much higher than the cost of the power generation cycle components; and (iii) the cost of generating electricity from the competing peak-demand power plants (e.g., CCGT) is higher than the cost of generating electricity from the heat storage system and the combustion heat source. Furthermore, Borowiec et al. [32] performed a simple analysis exploring the potential economic benefits of running a 3.5 GW_{th} nuclear reactor coupled with a TES system in different electricity markets in the USA. Different market scenarios based on the shares of VRES (i.e., wind and solar) and different capacity prices were tested. It was found that profitability could be achieved but it highly depends on: (i) the share of VERS; (ii) the type of electricity markets; (iii) the installed capacity; and (iv) the material and installation costs of the TES system.

The present work goes beyond previous research by: (i) developing and exploring load-following operations via secondary ORC power plants coupled to the TES assets; and (ii) investigating the economic feasibility of such flexible generation solutions integrated to virtual power plant operation, accounting for both investment costs and revenues, all while considering the design of different configurations for integrating TES and ORC plants in a currently operating nuclear power plant, and actual electricity price variations in the UK. In more detail, we attempt to:

- Design a selection of different configurations for integrating TES and secondary ORC plants in a currently operating nuclear power plant in the UK.
- Understand the variations to the performance and operation of baseload power plants from a thermodynamic perspective when integrating different TES strategies (Sections 3 and 4), and to quantify the potential variations in generation capacity between peak and off-peak times.
- Identify and discuss the advantages of using PCMs in TES systems, considering the choice of suitable materials and how this affects the performance and operation of the whole EMS.
- Account for the performance and capital cost of the secondary ORC generators that later converts the stored thermal energy to electricity.
- By means of an economic analysis (Section 4.2), proceed finally to estimate the potential profits that can result from the operation of the proposed EMS in light of the expected rewards from flexible generation and different TES-ORC sizing criteria.

2. Concept description

Fig. 1 presents an outline of the main components of the power plant under investigation, which is an advanced gas-cooled reactor (AGR) nuclear power plant operated by a Electricite de France (EdF) in the UK. The corresponding thermodynamic processes are shown on a temperature-specific entropy (*T–s*) diagram in Fig. 1b.

Referring to Fig. 1, the working fluid undergoes the following processes [41,42]:

- *Process 1–2*: Expansion of the steam through the high-pressure turbine (HPT);
- *Process 2–3*: Isobaric heat addition to the steam through the reheater;

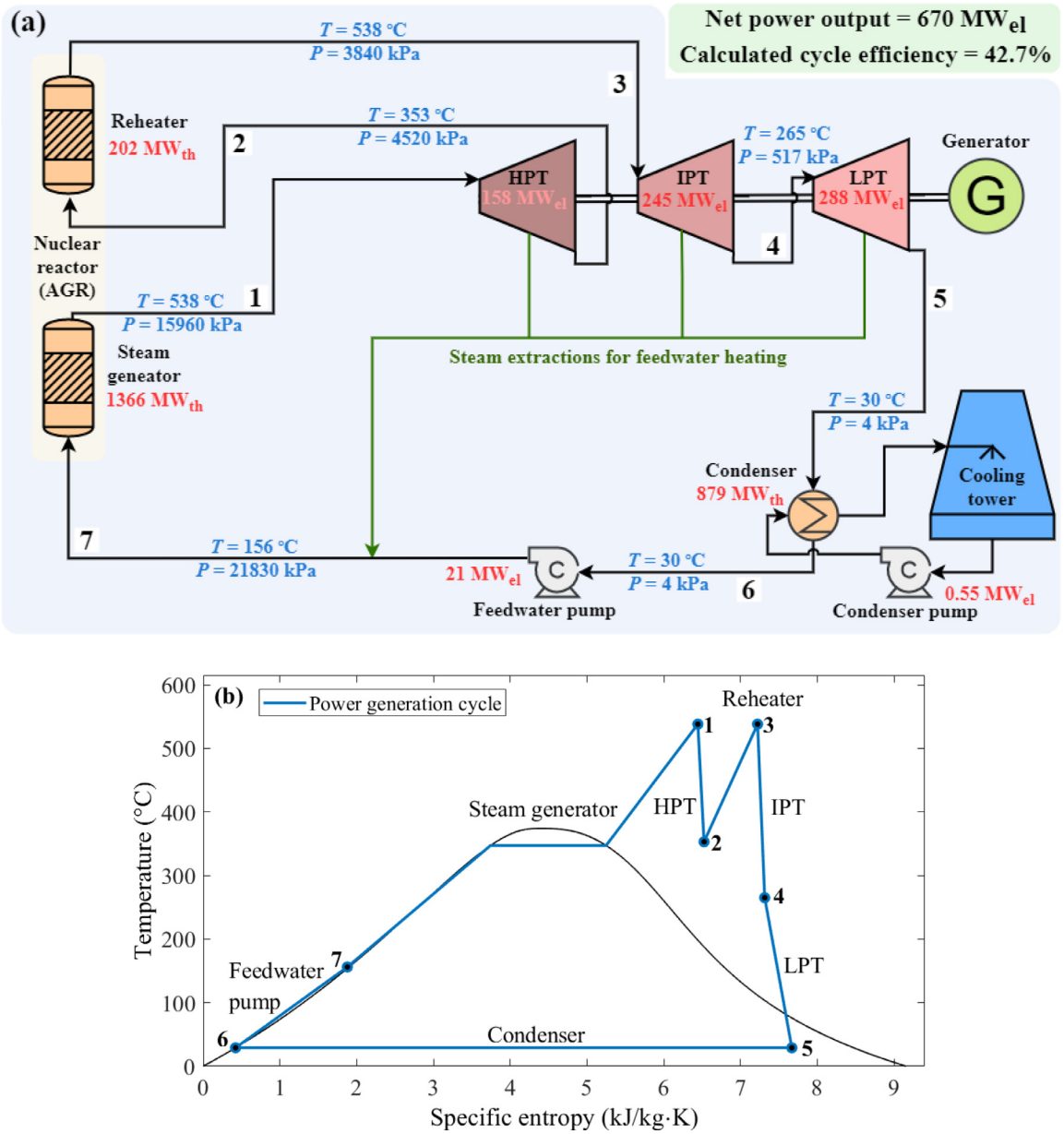

Fig. 1. (a) Layout of the nuclear power plant considered as a case study in this work, and (b) the corresponding Rankine cycle on a thermodynamic *T–s* diagram. For simplicity, multiple bleed points from the turbines for regenerative feed heating are denoted in this figure by a single line connecting the turbines to the output of the feedwater pump.

- *Process 3–4*: Expansion through the intermediate-pressure turbine (IPT);
- *Process 4–5*: Expansion through the low-pressure turbine (LPT) to the condenser pressure;
- *Process 5–6*: Heat transfer from the steam at constant pressure through the condenser with saturated liquid at State 6;
- *Process 6–7*: Pressurisation of the saturated working fluid (liquid) in the feed pump;
- *Process 7–1*: Isobaric heat addition to the working fluid as it flows at constant pressure through the steam generator to complete the cycle.

The thermal input to the power plant is 1570 MW_{th}, the electrical power output is 670 MW_{el} and the electric efficiency at rated power is 43%. The isentropic efficiencies of the high-, intermediate- and low-pressure turbines are 85%, 92% and 85%, respectively. The electrical power consumption of the feed pump is 21 MW_{el} and its isentropic efficiency is 74%.

We consider the integration of TES with the aim of modulating the plant's electrical power output, as illustrated in the example in Fig. 2. At base conditions, the power output of the plant is constant at the plant's rated power (i.e., at 670 MW_{el}; horizontal line in Fig. 2). In our proposed EMS, the power plant operator is informed, e.g., one day ahead, of the hourly electricity-exchange prices in the transmission network. An automated EMS then makes decisions for the charging-discharging of the TES stores by solving the unit commitment problem.

As an example, Fig. 2 illustrates a scenario in which the thermal tanks are charged twice per day, at 3 am and 1 pm (signified by dips in the shaded area). The tanks are coupled to and provide thermal energy to secondary ORC power plants, and such plants are shown here indicatively as producing approximately 152 MW_{el} of electrical power during peak demand, which is lower than the stored heat due to the ORC heat-to-electricity conversion losses. The TES tanks are discharged at 8 am

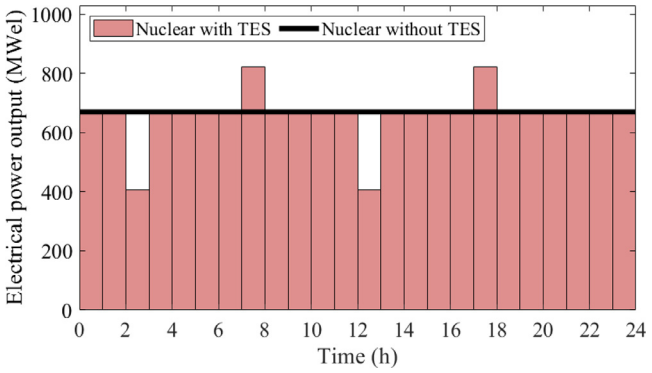

Fig. 2. Baseline net electrical energy production from the EdF nuclear power plant (670 MW_{el}) and electrical energy production after integration of the TES system. Note derating of power plant and peak capacity exceeding the baseline value due to the contribution of the power generated by the secondary bottoming cycles as part of the TES system in addition to the main power plant.

and 6 pm (peaks in the shaded area). Such a scenario with flexible operation of power plants, in response to the hourly electricity prices, can play a crucial role in the accelerated penetration of renewable energy sources into the grid. In particular, these TES-ORC systems can be considered autonomous units which could be connected to a virtual power plant providing flexible generation or participating to ancillary services markets.

3. Power plants with integrated thermal energy storage

The charging characteristics of thermal energy stores depend strongly on the materials and on the temperature at which steam is extracted from the nuclear power plant. Following consultation with EdF, we consider the possibilities that steam can be extracted: (i) before the reheater at 353 °C and 4.52 MPa; and/or (ii) before the LPT at 265 °C and 517 kPa.

The design of the TES tanks is based on shell-and-tube heat exchangers, with the steam condensing as it flows through the tubes and suitable PCMs used in the shells. In both of the above cases, the steam comes into contact with the inner surfaces of the tubes, whose temperatures are below its condensation temperature. Therefore, the design of the TES tanks becomes essentially the design of steam condensers. Several methodologies have been proposed in the literature for designing such condensers [43]. Here we assume that the conditions (i.e., mass flowrate, diameter) are such that downwards annular flow is established in the tubes [44–46]. This flow regime permits complete wetting of a tube's inner surfaces, such that the steam does not condensate directly on the solid wall but over the surface (interface) of a liquid film [46].

3.1. TES integration–Charging with steam extraction before reheater

In this scheme, illustrated in Fig. 3, the steam undergoes the following processes:

- *Process 2-a*: Diversion of part of the working fluid (superheated steam) flow upstream of the reheater followed by isobaric heat rejection and condensation of the steam flow while charging a first PCM thermal-tank (Thermal Tank 1);
- *Process a-b*: Isobaric heat rejection of the working fluid (water) while charging a second PCM thermal-tank (Thermal Tank 2);
- *Process b-7*: Pressurisation of the subcooled working fluid (water) in a feed pump and return of the diverted flow to the main plant steam generator.

As a guideline for this particular power plant, EdF has provided with an allowable steam-extraction rate of up to 54 kg/s for diversion from the reheater to Thermal Tank 1 (and also Thermal Tank 2, which is in series with the first tank; see Fig. 3). This represents 12% of the total steam passing to the reheater under normal conditions. As a result, thermal energy can be stored in Thermal Tank 1 at a maximum heat transfer rate of 107 MW_{th} and in Thermal Tank 2 at a rate of 26 MW_{th} during charging.

Superheated steam at 353 °C (and 4.52 MPa) is extracted before the reheater and condensed isobarically to a stream of saturated liquid water at 258 °C (4.52 MPa). The storage medium in this tank is a PCM mixture of sodium nitrate and sodium hydroxide (86 wt% $NaNO_3$ + 14 wt% NaOH) with a melting point of 250 °C [47], which is just below the minimum temperature of the steam in the tank. We assume that pure steam enters the pipes of Thermal Tank 1 at a relatively high velocity and that a uniformly thin condensate film forms around the pipe surface. At the output of the tank the steam is separated from the water in a steam drum and recirculated through the condenser [48]. Of great importance in the implementation of such scheme is the space (i.e., volume) required for the installation of the storage tanks that form the core part of this TES system. The procedure used for the design of Thermal Tank 1 is detailed in Appendix A.1 and is based on the methodology described in Ref. [46]. A summary of results relating to the sizing of this heat-exchanger/tank is provided in Table 1.

Downstream, and in series with Thermal Tank 1, heat transfer also occurs to Thermal Tank 2 where the condensed, high-pressure (initially saturated) water-stream cools further, again isobarically as it charges this second tank. The inlet temperature of this tank is 258 °C (at 4.52 MPa) and the outlet temperature is 154 °C (at 4.52 MPa). This tank employs a salt mixture referred to as HITEC (composition: 7 wt% $NaNO_3$+53 wt% KNO_3+40 wt% $NaNO_2$) with a melting point of 142 °C [49,50], which is (as in Thermal Tank 1) just below the minimum temperature in this tank. The approach used for the design of Thermal Tank 2 is based on the single-phase Gnielinski correlation for condensed water flows, assuming a constant tube surface temperature [51], as summarised in Appendix A.2. Corresponding results are presented in Table 1.

Finally, after the two TES tanks, the subcooled liquid (water) is compressed in a feed pump and returned to the steam generator/reactor. The electrical power consumption of the additional feed pump is estimated at 1.23 MW_{el}, by using an isentropic efficiency value of 80% for this component. The partial diversion of the steam flow to the reheater during the charging of the two cascaded thermal tanks leads to a drop in the thermal input of the power plant from 1570 MW_{th} to 1540 MW_{th}, and the electrical power output of the power plant is derated by 9.4% (from 670 MW_{el} to 607 MW_{el}) and the corresponding thermal efficiency of the plant decreases from 43% to 39%.

3.2. TES integration–Charging with steam extraction before LPT

Fig. 4 depicts the integration of PCM-based TES in an arrangement whereby steam is extracted before the LPT along with its associated *T–s* diagram. In this scheme, the working fluid (steam) undergoes the following processes:

- *Process 4-c*: Diversion of part of the working fluid (superheated steam) flow upstream of the LPT followed by isobaric heat rejection and condensation of the steam flow while charging a third PCM thermal-tank (Thermal Tank 3);
- *Process c-7*: Pressurisation of the saturated working fluid (water) in a feed pump and return of the diverted flow to the steam generator.

Superheated steam at 265 °C (and 517 kPa) is extracted after the intermediate-pressure turbine and before the LPT, and is condensed isobarically in horizontal tubes in Thermal Tank 3 to a stream of saturated liquid water at 153 °C (and 517 kPa). HITEC is again selected as the storage material for Thermal Tank 3, with a melting temperature of 142 °C. As above in Section 3.1, we are interested in the space requirements for the installation of Thermal Tank 3 as part of this TES scheme. The methodology outlined in Appendix A.1 in relation to the design and siz-

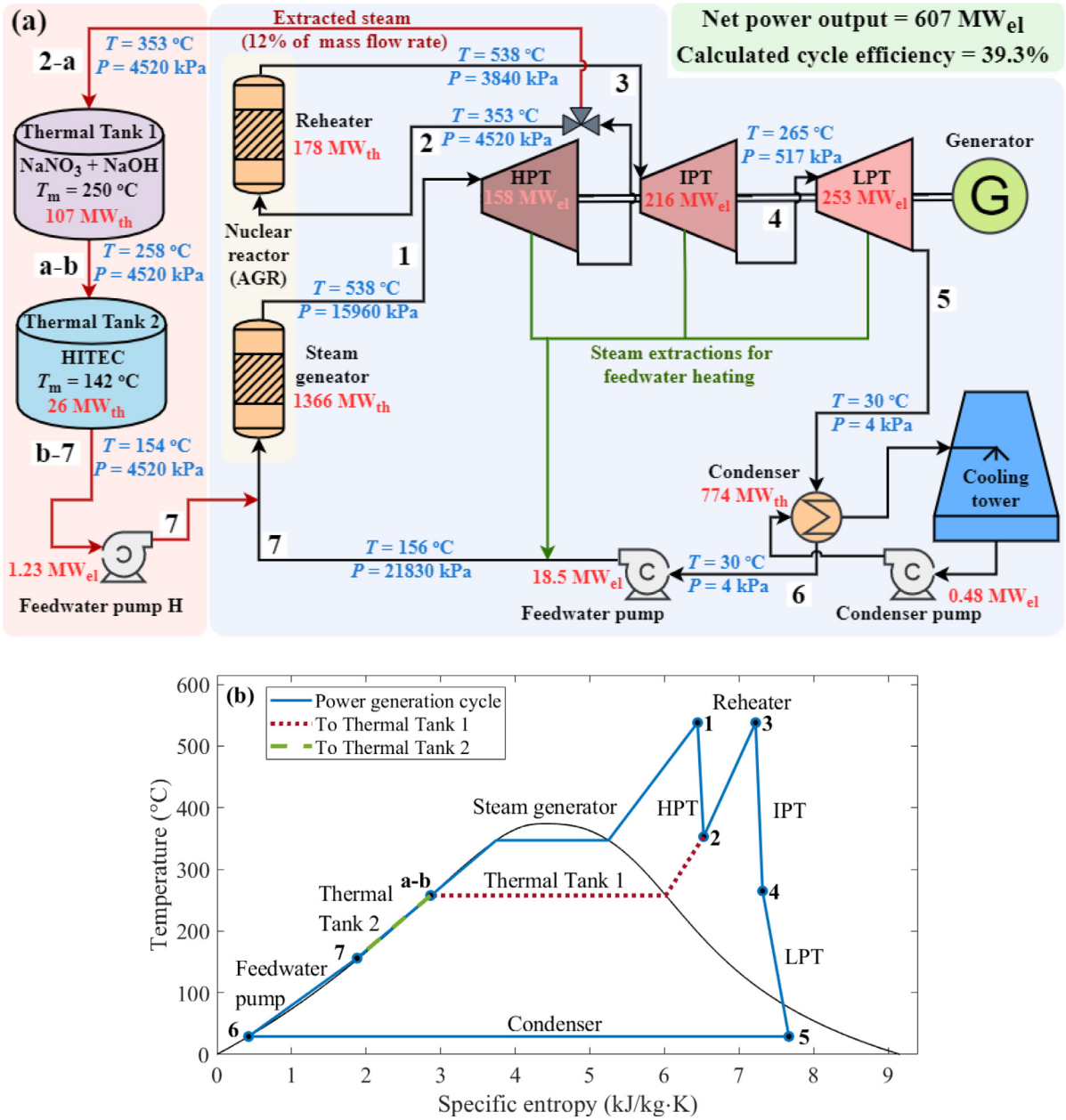

Fig. 3. (a) Layout of the nuclear power plant integrated with two PCM-based TES tanks that are charged with steam extracted before the reheater, and (b) the corresponding Rankine cycle on a thermodynamic *T*–*s* diagram. For simplicity, multiple bleed points from the turbines for regenerative feed heating are denoted in this figure by a single line connecting the turbines to the output of the feedwater pump.

ing of Thermal Tank 1 (see Section 3.1) is also adopted for the design of Thermal Tank 3. The results are summarised in Table 1.

For the case study considered in this work, EdF has provided with a maximum allowable steam extraction rate of 383 kg/s for diversion from (i.e., before) the LPT to Thermal Tank 3, which represents 80% of the total steam flow to the turbine under normal conditions. The corresponding heat transfer rate during charging of the tank is 899 MW_{th}. Furthermore, during the charging of Thermal Tank 3, the thermal input to the power plant is unchanged from the nominal value of 1570 MW_{th}, and its electrical power output is derated by 34% to 443 MW_{el} as its thermal efficiency reduces to 28%. The electrical power consumption of the pump is 13.6 MW_{el}, again based on an isentropic efficiency of 80% as in the scheme in Section 3.1.

3.3. TES integration–Charging with steam extraction before reheater and LPT

In this scheme, the two combined TES systems are considered; steam is extracted before the reheater (as in Section 3.1) and before the LPT (as in Section 3.2). Due to the steam extraction before the reheater, the minimum allowable steam flowrate through the LPT, which must still be 80% of the remaining steam after the reheater, is now reduced to 337 kg/s, and the heat transfer rate to Thermal Tank 3 is now reduced to 792 MW_{th}. Fig. 5 shows the combined TES system and its *T*–*s* diagram. Based on the sizing criteria described in Sections 3.1 and 3.2 and detailed in Appendix A, the technical details of the three thermal tanks are summarised in Table 1.

Table 1
Summary of thermal tank designs: dimensions, material properties and other relevant input parameters. Heat storage capacity is referred to thermal storage charging time of 1 h [47,49,50,52].

Thermal tank number (orientation)	Thermal Tank 1 (horizontal)	Thermal Tank 2 (vertical)	Thermal Tank 3 (horizontal)
Phase-change material	$NaNO_3$+NaOH	$NaNO_3$+KNO_3+$NaNO_2$ (HITEC)	
Melting temperature (°C)	250	142	
Latent heat of fusion (kJ/kg)	160	81.4	
Density (kg/m^3)	2240, 1980*	$\rho = -0.733\theta + 2080^{\dagger}$	
Specific heat capacity (kJ/kg·K)	1.19, 1.86*	$c_p = 1.56 - (\theta/1000)^{\dagger}$	
Thermal conductivity (W/m·K)	0.66, 0.60*	$k = (2\times10^{-6})\,\theta^2 - (4\times10^{-4})\,\theta + 0.558^{\dagger}$	
Total steam mass flowrate (kg/s)	54	54	337
Heat transfer rate (MW_{th})	107	26	899
Heat storage capacity (GJ)	385	92	3240
Storage density (MJ/m^3)	453	165	165
Volume (m^3)	850	557	19,600
Sensible/total heat ratio (%)	20.8	100	10.3
Length (m)	120	–	245
Width (m)	3	–	7
Height (m)	4	17	17
Diameter (m)	–	6.5	–

* First value is for the solid and the second for the liquid phase. $^{\dagger}\theta$ is the PCM bulk temperature in °C.

3.4. TES integration–Charging, discharging and implications for cascaded tank design

Generally, the overall exergy efficiency associated with the charging and discharging of TES tanks is lower when exploiting latent-heat (PCM) storage compared to sensible-heat storage and the heat-source temperature is variable (e.g., when storing the sensible enthalpy of a hot fluid stream in the absence of phase change) [45,46]. However, the generation-integrated energy storage solutions proposed here consider a heat-source temperature that is, to a large extent, constant during the storage-tank charging phase, and furthermore, the stored thermal energy is used later, i.e., during discharge, to drive secondary power plants (ORC systems) by boiling an organic working fluid, again at constant temperature. This makes latent (PCM-based) TES an interesting alternative with trade-offs necessary for achieving the maximum ("round-trip") efficiency of the overall system. Furthermore, beyond efficiency considerations, it can be argued that affordability is an even more desirable performance indicator, e.g., with larger temperature differences between the heat source and the material in the thermal store (up to a point) leading to smaller heat transfer areas (i.e., sizes) and costs, even though the thermodynamic performance is lower.

The appropriateness of using a single PCM-based (latent) thermal store from the point of view of the exergy efficiency of the charging and discharging processes is clear for isothermal heat sources and sinks. The presence of temperature variations can be addressed by increasing the number and respective phase-change temperatures of the thermal storage tanks, in so-called 'cascaded' tanks, which allows one to control the exergy losses in the charging/discharging processes. In the theoretical limit of an infinite number of ideal (zero temperature-difference between the tanks and heat source) cascaded infinitesimal thermal tanks, each featuring a different PCM with a suitable phase-change temperature, this allows an exergetically optimal latent TES solution similar to a perfectly matched sensible thermal-energy store. In this case, the melting points of the PCMs must be chosen to match the temperature variation of the heat transfer fluid (heat source). Fig. 6 illustrates this concept of cascaded TES tanks. This theoretical case, however, is not a practically feasible or economically viable solution, although it is of interest in setting an upper limit to overall thermodynamic performance. In this work, we consider the case of TES when using a single or a cascade of two PCM tanks in series as one solution in dealing with the aforementioned heat-source temperature variations. In future work, we intend to investigate additional cases, but the present approach suffices in describing our proposed concept for integrating PCM-based TES tanks into power plants along with secondary power generation at a reasonable cost.

Assuming a negligible temperature difference between the heat source and the PCM in a TES tank, the maximum useful stored power $\dot{W}$ during the charging of this tank is the rate change of exergy of the heat-source stream, which can be isothermal or experience temperature variations:

$$\dot{W} = \Delta\dot{H} - T_d\Delta\dot{S} = \begin{cases} \dot{Q} - \dot{m}\,T_d\,\Delta s; & \text{for isothermal source} \\ \dot{Q} - \dot{m}c_pT_a\,\ln\left(\frac{T_{in}}{T_{out}}\right); & \text{for temperature – varying source} \end{cases} \quad (1)$$

where $\dot{H}$ and $\dot{S}$ are the enthalpy and entropy (rates) of both the heat-source stream and PCM in the tank, $\dot{m}$ and c_p are the heat-source stream mass flowrate and specific heat capacity, T_{in} and T_{out} are the inlet and exit temperatures of the stream to/from the tank when its temperature is varying, and $T_d = T_a$ is the dead-state temperature that is taken here to be the ambient temperature (T_a = 25 °C).

3.5. TES integration–Discharging with secondary power plants

The stored heat is discharged to generate electrical power using secondary power plants, specifically two ORC engines at different temperature levels depending on the temperature of the PCM storage tanks. The main reason of selecting regenerative ORC systems in this study is their capability to operate at low temperature range (less than 250 °C) with higher heat-to-electricity conversion efficiency compared to steam cycles [53].

Figs. 7 and 8 show the schematics of the proposed systems ORC-1 and ORC-2, respectively. System ORC-1 is coupled to Thermal Tank 1 and Thermal Tank 2, while system ORC-2 is coupled to Thermal Tank 3. Both ORC systems contain the following:

- two PCM tanks for heat addition (i.e., Thermal Tank 1 and Thermal Tank 2) for system ORC-1 and one PCM tank (Thermal Tank 3) for system ORC-2;
- an expander (i.e., turbine) with one side extraction for feed heating;
- a water-cooled condenser with a cold stream temperature of 25 °C;
- two pumps (condensate and feed pump); and,
- an internal heat exchanger to preheat the organic working fluid before evaporation.

In system ORC-1, the organic working fluid is evaporated by a constant temperature heat addition (T = 142 °C) from Thermal Tank 1 and then superheated, also at a constant temperature (T = 250 °C) but from Thermal Tank 2. In system ORC-2, the selected organic working fluid is evaporated and superheated at constant temperature of heat addition (T = 142 °C) from Thermal Tank 3.

The power cycles of both ORC systems are computationally simulated using MATLAB and all working fluid properties are obtained using

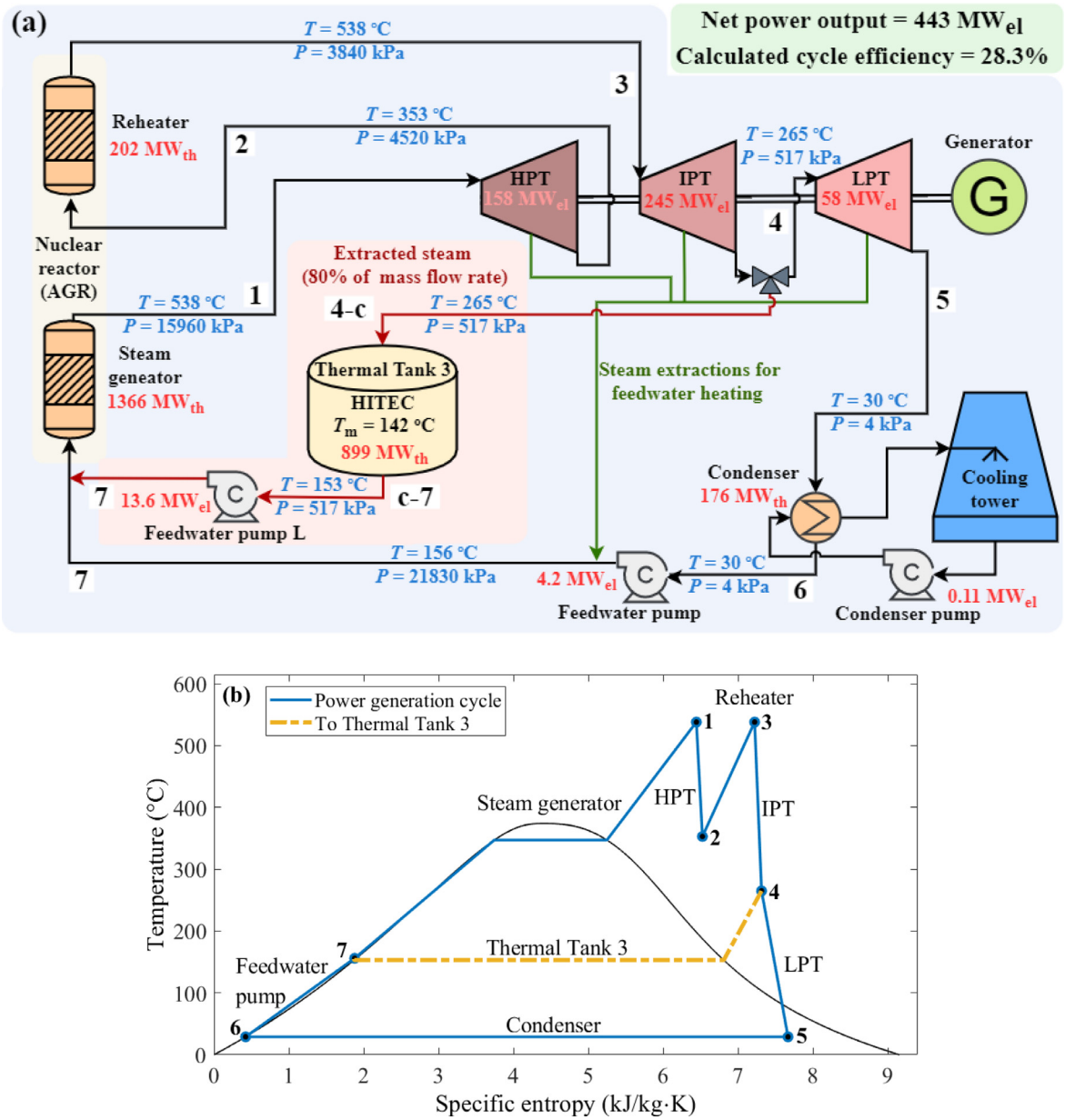

Fig. 4. (a) Layout of the nuclear power plant integrated with one PCM-based TES tank that is charged with steam extracted before the LPT, and (b) the corresponding Rankine cycle on a thermodynamic *T*–*s* diagram. For simplicity, multiple bleed points from the turbines for regenerative feed heating are denoted in this figure by a single line connecting the turbines to the output of the feedwater pump.

REFPROP function [54]. The thermodynamic parameters are selected to maximise the heat-to-electricity efficiency of the ORC, giving maximum electrical power output for a fixed amount of heat input. The ORC efficiency optimisation function is:

$$\max_{T_{FP},\dot{m}_{ORC},\dot{m}_{SE},P_{evap},P_{SE},P_{CP}} \{\eta_{ORC}\} \tag{2}$$

where η_{ORC} is the ORC heat-to-electricity efficiency, T_{FP} the feed pump outlet temperature, $\dot{m}_{ORC}$ the cycle mass flowrate, $\dot{m}_{SE}$ the turbine side extraction mass flowrate, P_{evap} the cycle evaporation pressure, P_{SE} the turbine side extraction pressure, and P_{CP} the condensate pump outlet pressure.

The rate of heat addition in all thermal tanks is:

$$\dot{Q}_{TT} = \eta_{TT}\,\dot{m}_{ORC}\,(h_{out} - h_{in}) \tag{3}$$

where $\dot{Q}_{TT}$ is the rate of added heat from a specified thermal tank, η_{TT} the thermal tank heat-to-heat efficiency, h the specific enthalpy of the working fluid, and subscripts 'in' and 'out' indicate the conditions at inlet and outlet of the thermal tanks.

The generated power by (each) turbine and needed power by (each) pump are calculated from:

$$\dot{W}_T = \dot{m}\,(h_{in} - h_{out}) \tag{4}$$

$$\eta_T = \frac{(h_{in} - h_{out})}{(h_{in} - h_{out,is})} \tag{5}$$

$$\dot{W}_P = \dot{m}\,(h_{out} - h_{in}) \tag{6}$$

$$\eta_P = \frac{(h_{out,is} - h_{in})}{(h_{out} - h_{in})} \tag{7}$$

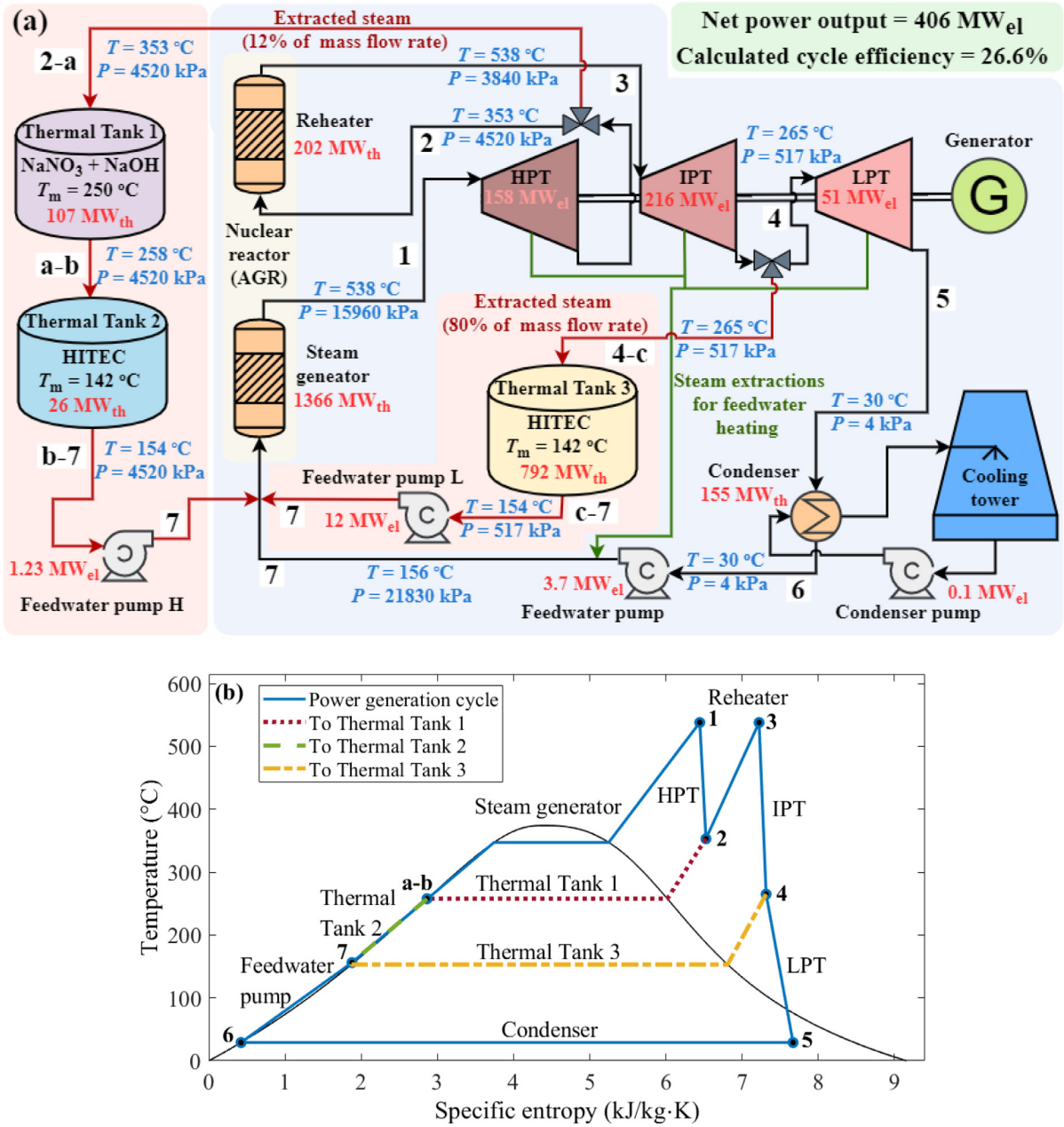

Fig. 5. (a) Layout of the studied nuclear power plant integrated with three PCM-based TES tanks that are charged with steam extracted before the reheater and before the LPT, and (b) the corresponding Rankine cycle on a thermodynamic *T–s* diagram. The dashed lines in the *T–s* diagram represent the thermodynamic process of depositing heat into the TES thermal tanks. For simplicity, as in the previous Figs. 3 and 4, multiple bleed points from the turbines for regenerative feed heating are denoted by a single line connecting the turbines to the output of the feed pump.

where $\dot{W}_T$ and η_T are the turbine power and isentropic efficiency, $\dot{W}_P$ and η_P the pump power and isentropic efficiency, and subscript 'is' indicates properties evaluated at equivalent isentropic conditions.

The total net generated power and net thermal efficiency of the ORC plants are:

$$\dot{W}_{net} = \sum \eta_G \dot{W}_T - \sum \dot{W}_P \tag{8}$$

$$\eta_{ORC} = \frac{\dot{W}_{net}}{\dot{Q}_{TES}} \tag{9}$$

where η_G is the generator efficiency and $\dot{Q}_{TES}$ the total heat rate input from thermal tanks.

The optimisation function is solved with the following set of non-linear constraints:

$$P_{cond} \geq 101.3 \text{ kPa} \tag{10}$$

$$T_{cond} \geq 25°C \tag{11}$$

$$P_{evap} \leq 0.95 P_{crit} \tag{12}$$

$$x_{CP} \leq 0 \tag{13}$$

$$x_{FP} \leq 0 \tag{14}$$

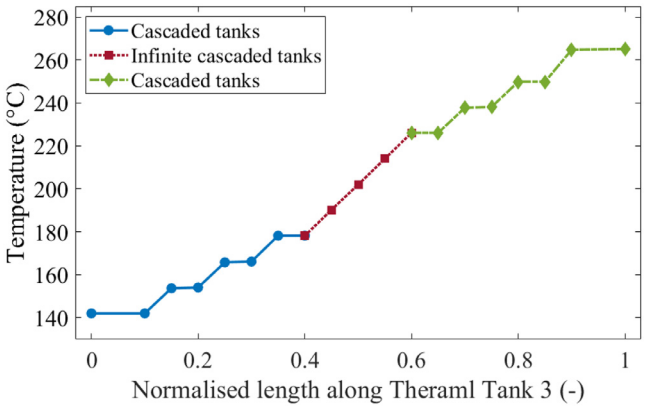

Fig. 6. Series of (theoretical) varying PCM thermal storage temperatures during charging when a series of cascaded thermal tanks is used in place of the single-PCM (HITEC) Thermal Tank 3. Note that we are only showing here a finite number of stores for the purposes of illustration.

$$\Delta T_{PP,IHX} \geq 10°C \tag{15}$$

$$T_{TT-1} \leq 142°C \tag{16}$$

$$T_{TT-2} \leq 250°C \tag{17}$$

$$T_{TT-3} \leq 142°C \tag{18}$$

where P_{cond} and T_{cond} are the condensation pressure and temperature, P_{evap} the evaporation pressure, P_{crit} the critical pressure of the working fluid, x_{CP} and x_{FP} the working fluid quality at condensate pump and feed pump outlet, respectively, $\Delta T_{PP,IHX}$ the pinch point temperature difference of the internal heat exchanger, and $T_{TT-1}, T_{TT-2}, T_{TT-3}$ the working fluid temperature at the outlet of Thermal Tank 1, Thermal Tank 2, and Thermal Tank 3, respectively.

The evaporation pressure upper bound is set at $0.95 P_{crit}$ to maintain the cycle in the subcritical region, as well as to reduce the capital costs of the ORC since components that withstand higher pressure are more expensive. All optimisation tasks are solved using MATLAB's non-convex interior point algorithm *fmincon* or genetic algorithm function *ga* within a specified set of upper and lower bounds.

The selection of the organic working fluid has a crucial impact on the thermal performance of the ORC. There is a wide range of organic fluids that could be selected but not all of them are considered or analysed in this paper. For system ORC-1, the heat source temperature is higher (i.e., up to 250 °C). Therefore, different group of organic working fluids, mostly hydrocarbons, that have higher critical temperature and pressure are suggested to maintain the ORC within the subcritical range [55,56]. For system ORC-2, several refrigerants and short-chained alkanes are suggested and listed in Table 2. These fluids are commonly used in commercial ORC power plants with similar heat source temperature range (e.g., geothermal power plants) [55]. The thermodynamic, environmental and safety characteristics of the considered working fluids are reported in Table 2.

Table 3 summarises the main assumptions of the computational model for both ORC systems. The heat capacity of all thermal tanks is based on the maximum charging scenario, as per Fig. 5. It is assumed that the heat-to-heat efficiency during discharging is 90%

Fig. 9 shows the maximum cycle thermal efficiency, on the left *y*-axis, and the optimal evaporation and condensation pressure, on the right *y*-axis, of the candidate working fluids for: a) system ORC-1, and b) system ORC-2. In system ORC-1, the results show that R11 has the highest cycle efficiency (i.e., 21%) at an optimal evaporation pressure of 4.19 MPa. Toluene has the lowest efficiency since its critical temperature is the highest amongst the other candidates and also much higher than the temperature of heat addition. In system ORC-2, the optimised cycle efficiency ranges between 14% and 16% depending on the type and the thermodynamic properties of the working fluid. The results show that isopentane not only gives the highest maximum cycle efficiency (i.e., 16%) at the specified constraints, but also the lowest evaporation pressure (1.73 MPa) which minimises the capital cost of the ORC power plants. Therefore, R11 and isopentane are selected as the working fluids for systems ORC-1 and ORC-2, respectively.

To obtain the optimal operating conditions of both ORC systems (i.e., mass flowrate, temperature, pressure, etc.) for each streamline in the power cycle, the input heat rates of all thermal tanks have to be determined, which depend on the total discharging duration of heat. For example, if the discharging duration for fixed heat capacity thermal tanks is doubled (from 1 h to 2 h), the discharging heat rate is now halved as the same amount of heat is discharged for longer duration, which corresponds to a reduced electric power capacity from the ORC systems. Therefore, different discharging cases based on the discharging duration and heat rate are introduced and listed in Table 4.

For each discharging case, the optimal ORC operating parameters that give the maximum thermal efficiency are calculated and reported in Table 5 for system ORC-1 and in Table 6 for system ORC-2. The main difference between the discharging cases is the ORC mass flowrate as it decreases with the increase of discharging duration, which also affects the ORC installed power. The maximum cumulated power outputs from

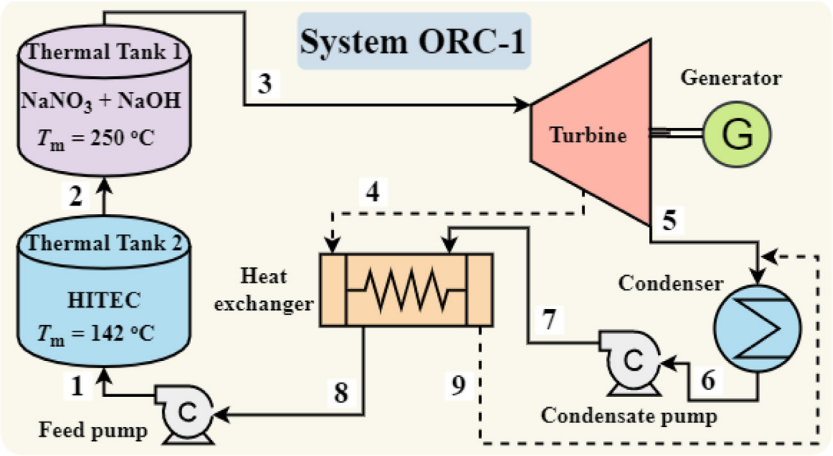

Fig. 7. Schematic of regenerative system ORC-1 operated by discharging stored heat from Thermal Tank 1 and Thermal Tank 2.

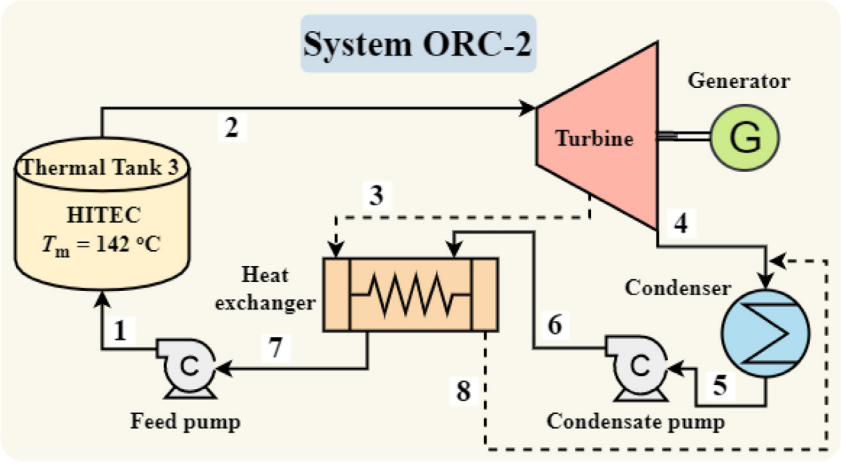

Fig. 8. Schematic of regenerative system ORC-2 operated by discharging stored heat from Thermal Tank 3.

Table 2
Summary of the main thermodynamic, environment and safety properties of the selected organic working fluids for systems ORC-1 and ORC-2 [55–60].

ORC system	Working fluid	Critical T (°C)	Critical P (kPa)	Boiling point (°C)	GWP	ODP	Flammability
ORC-1	Acetone	235	4690	56.1	Low	0	Flammable
	Benzene	289	4890	80.1	Low	0	Flammable
	Cyclohexane	280	4080	80.7	Low	0	Flammable
	R11	198	4410	23.8	1500	0	Non-flammable
	R141b	204	4210	32.1	725	0.12	Non-flammable
	Toluene	319	4130	111	Low	0	Flammable
ORC-2	Isobutane	135	3630	−11.7	Low	0	Flammable
	Isopentane	187	3380	27.8	Low	0	Flammable
	R123	184	3670	27.6	Low	0.06	Non-flammable
	R1233zd	166	3570	18.3	Low	0	Non-flammable
	R245fa	154	3650	15.1	1030	0	Non-flammable

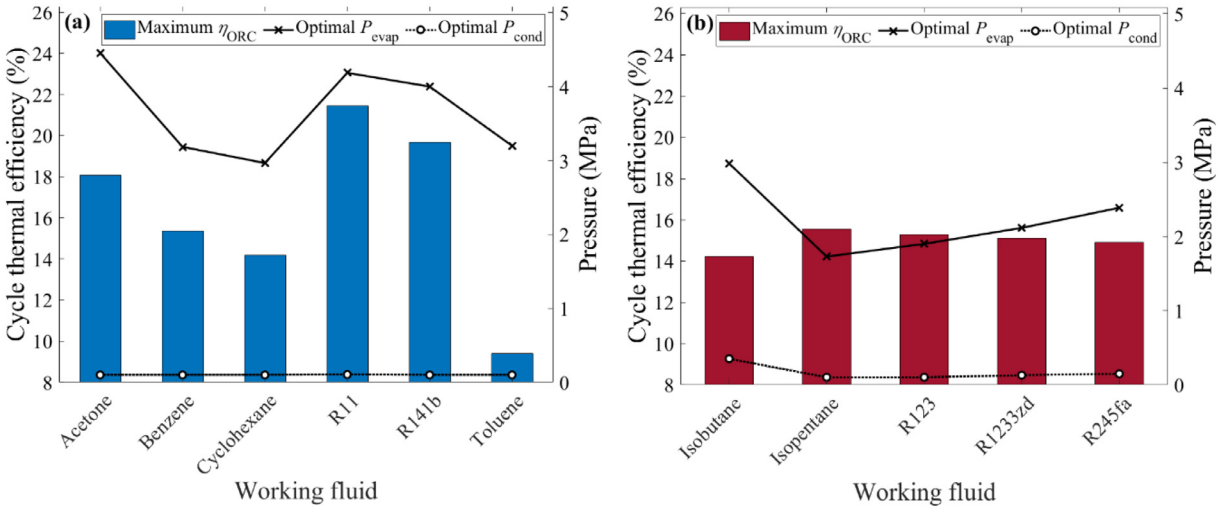

Fig. 9. Maximum cycle thermal efficiency, on the left *y*-axes, along with corresponding optimal evaporation and condensation pressure, on the right *y*-axes, of the compared organic working fluids for system: (a) ORC-1, and (b) ORC-2.

both the first and the second ORC systems are 152 MW_{el} for Case A, 75.8 MW_{el} for Case B, 37.5 MW_{el} for Case C, and 19 MW_{el} for Case D. Yet, the amount of the total electricity generated for a full discharging phase from the two ORC systems is the same for all cases (152 MWh per full discharge).

Fig. 10 illustrates the charging and the discharging behaviour of the EMS for the proposed discharging cases for an arbitrary day in the UK, including all thermal tanks and the two ORC generators. The left *y*-axes indicate the power output level, and the right *y*-axes report the whole-sale electricity prices during the same hour. The reported electricity price profile in Fig. 10 are actual prices of a randomly selected day in the UK in 2019 [61]. In all cases, the 1-h charging process is set to take place during the minimum price, which is at 4 am. Thus, the nuclear power unit generates the minimum rated power (406 MW_{el}) instead of nominal power (670 MW_{el}). The stored heat is then discharged during the maximum electricity prices (i.e., at 8 pm for Case A, from 7–8 pm for Case B, from 6–9 pm for Case C, and from 7–10 am and from 6–9 pm for Case D).

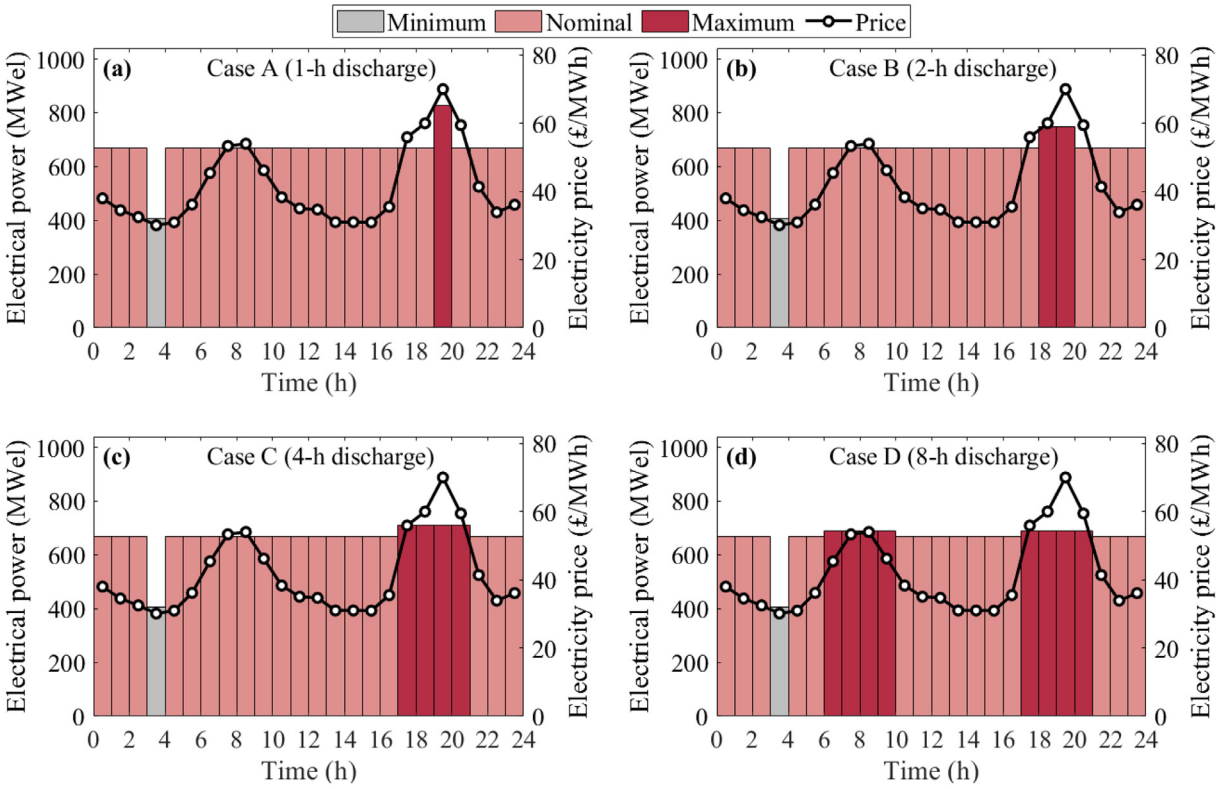

Fig. 10. EMS electrical power output, on the left *y*-axes, and wholesale electricity prices, on the right *y*-axes, for all discharging cases (A, B, C, and D). The minimum output power is when the EMS storing heat and the maximum is when the stored heat is discharged through the proposed ORC systems. The electricity price is the actual prices of a randomly selected day in the UK in 2019.

Table 3
List of main parameters assumed in both ORC system computational models.

Parameter/Assumption	Value
Thermal Tank 1 heat capacity (GJ)	385
Thermal Tank 2 heat capacity (GJ)	92
Thermal Tank 3 heat capacity (GJ)	2850
Thermal tanks heat-to-heat efficiency (%)	90
Turbine isentropic efficiency (%)	80
Turbine mechanical efficiency (%)	96
Pump isentropic efficiency (%)	75
Pump mechanical efficiency (%)	96
Generator electric efficiency (%)	95
Pressure loss in each thermal tank and in the heat exchanger (kPa)	100

Table 4
List of the proposed discharging cases.

Case	Full discharging duration (h)	Discharging heat rate (MW_{th})		
		Thermal Tank 1	Thermal Tank 2	Thermal Tank 3
A	1	26	107	792
B	2	13	53.5	396
C	4	6.5	26.8	198
D	8	3.3	13.4	99

Table 5
Optimal operating conditions for system ORC-1 using R11 as a working fluid.

Case (thermal tank discharging duration)	A (1 h)	B (2 h)	C (4 h)	D (8 h)
Thermal Tank 1 heat rate (MW_{th})	26	13	6.5	3.3
Thermal Tank 2 heat rate (MW_{th})	107	53.5	26.8	13.4
Turbine inlet mass flowrate (kg/s)	570	285	143	71.3
Turbine inlet temperature (°C)	231	231	231	231
Turbine side extraction pressure (kPa)	261	261	261	261
Turbine side extraction mass flowrate (kg/s)	176	87.8	43.9	21.9
Turbine side extraction temperature (°C)	112	112	112	112
Turbine main exhaust pressure (kPa)	106	106	106	106
Turbine main exhaust mass flowrate (kg/s)	395	197	98.6	49.4
Turbine main exhaust temperature (°C)	84.6	84.6	84.6	84.6
Condenser outlet temperature (°C)	25	25	25	25
Condenser outlet pressure (kPa)	106	106	106	106
Condensate pump outlet pressure (kPa)	4100	4100	4100	4100
Feed pump outlet pressure (kPa)	4190	4190	4190	4190
Feed pump outlet temperature (°C)	102	102	102	102
Net electric power from ORC-1 (MW_{el})	28.4	14.2	7.1	3.6
Gross amount of electricity (MWh)	28.4	28.4	28.4	28.4
Optimised cycle efficiency (%)	21.5	21.5	21.5	21.5
Total nuclear power with system ORC-1 (MW_{el})	698	684	677	674

The EMS behaviour for a two full charging/discharging cycles per day is presented in Fig. 11. The second 1-h charging phase is assumed to take place after a full discharge of the stored heat. For example, in Case A, the charging process is performed twice during the day at 4 am and 4 pm, where the two minimum prices are observed. However, the second charge phase does not start until all thermal tanks are fully discharged which occurs at 9 am where the electricity price is high. The same concept is applied for all the other cases.

3.6. Transient operation

Beyond the steady-state design of the thermal tanks considered above, it is necessary to account for the transient thermal performance of these tanks during charging and discharging in order to ascertain whether these processes are fast enough for the purposes of our EMS application. For the PCM in each thermal tank, we consider the energy balance equation (Eq. (19)) in which the change in the internal energy

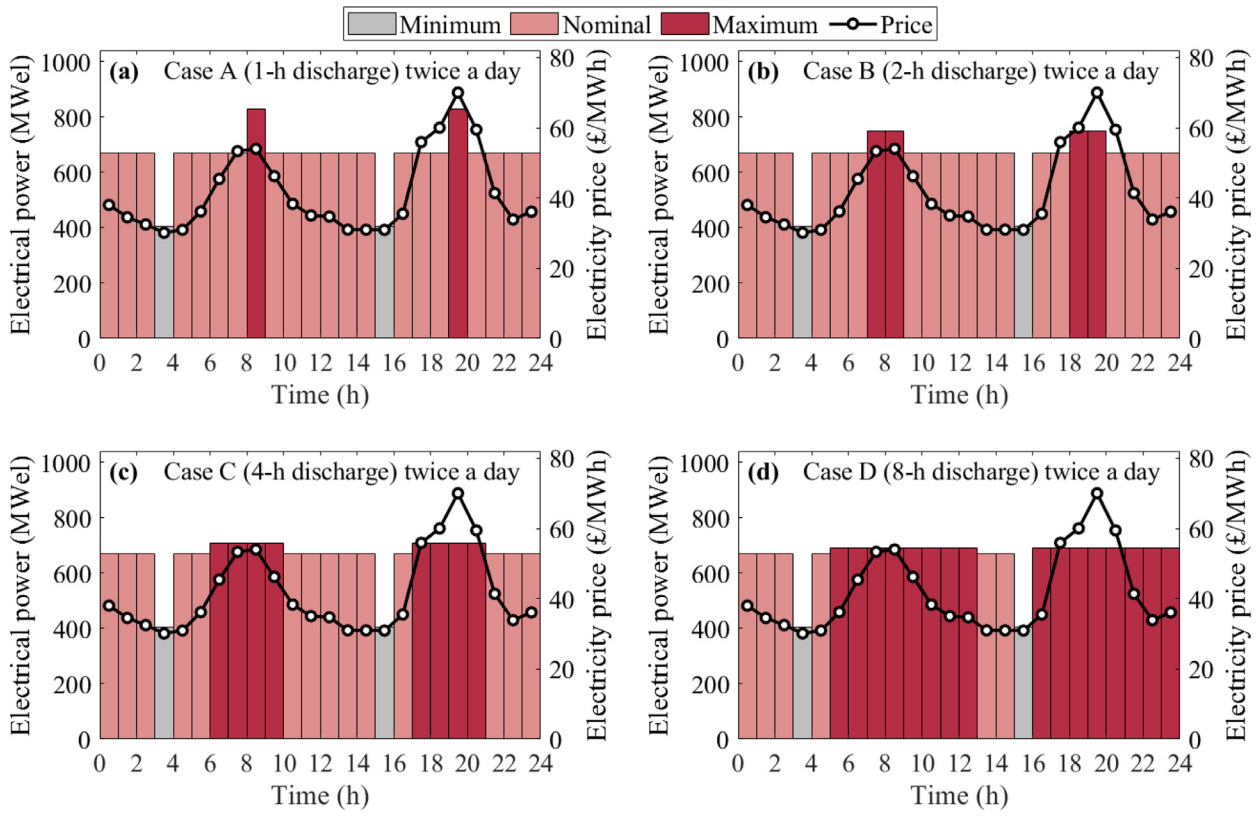

Fig. 11. EMS electrical power output, on the left *y*-axes, and the wholesale electricity prices, on the right *y*-axes, for all discharging cases (A, B, C, and D) for two charging/discharging cycles per day. The minimum output power is when the EMS storing heat and the maximum is when the stored heat is discharged through the proposed ORC systems. The electricity price is the actual prices of a randomly selected day in the UK in 2019.

Table 6
Optimal operating conditions for system ORC-2 using isopentane as a working fluid.

Case (thermal tank discharging duration)	A (1 h)	B (2 h)	C (4 h)	D (8 h)
Thermal Tank 3 heat rate (MW_{th})	792	396	198	99
Turbine inlet mass flowrate (kg/s)	1890	943	471	236
Turbine inlet temperature (°C)	142	142	142	142
Turbine side extraction pressure (kPa)	243	243	243	243
Turbine side extraction mass flowrate (kg/s)	582	291	146	72.7
Turbine side extraction temperature (°C)	93.2	93.2	93.2	93.2
Turbine main exhaust pressure (kPa)	101	101	101	101
Turbine main exhaust mass flowrate (kg/s)	1300	651	326	163
Turbine main exhaust temperature (°C)	76.7	76.7	76.7	76.7
Condenser outlet temperature (°C)	27.8	27.8	27.8	27.8
Condenser outlet pressure (kPa)	101	101	101	101
Condensate pump outlet pressure (kPa)	613	613	678	680
Feed pump outlet pressure (kPa)	1730	1730	1730	1730
Feed pump outlet temperature (°C)	84.1	84.1	84.1	84.1
Net electric power from ORC-2 (MW_{el})	123	61.6	30.8	15.4
Gross amount of electricity (MWh)	123	123	123	123
Optimised cycle efficiency (%)	15.6	15.6	15.6	15.6
Total power from nuclear and ORC systems (MW_{el})	822	746	708	689

of the PCM is equal to the net amount of energy transferred across the PCM control-volume boundary due to heat transfer over some time interval. This energy exchange can be both latent or sensible. Neglecting the tube walls in the thermal tanks, the temperature of the PCM in a thermal tank is obtained from the following first-order equation:

$$\dot{Q}_{TT} = \dot{m}\, c_p \left(T_{in} - T_{out}\right) = \bar{\alpha}\, A_s\, \Delta T_{LM} = \begin{cases} m_{PCM}\, c_{PCM}\, \frac{dT_{PCM}}{dt}; \text{ for sensible TES} \\ \Delta h_{PCM}\, \frac{dm_{PCM}}{dt}; \text{ for latent TES} \end{cases} \quad (19)$$

where $\dot{m}$ is the mass flowrate of steam in the tubes, c_p is the specific heat capacity of the steam, T_{in} and T_{out} are the inlet and outlet steam temperatures, $\bar{\alpha}$ is the average convection heat transfer coefficient, A_s is the total tube surface area, ΔT_{LM} is the log-mean temperature difference between the steam stream and the PCM. For sensible TES charging and discharging, m_{PCM} is the mass of the PCM in the tank, c_{PCM} is the specific heat capacity of the (solid or liquid) PCM, and $\frac{dT_{PCM}}{dt}$ is the rate of change of the PCM bulk temperature in the tank. During latent TES charging and discharging, thermal energy is used to induce phase change without a temperature variation for pure substances, and the final term in Eq. (19) becomes $\Delta h_{PCM} \frac{dm_{PCM}}{dt}$ where Δh_{PCM} is the PCM specific phase-change enthalpy, and $\frac{dT_{PCM}}{dt}$ is the rate at which PCM mass changes phase.

Fig. 12 shows, as an example, the bulk temperature variation of the PCM in Thermal Tank 3 during charging following Eq. (19). The HITEC is initially in the solid phase at ambient temperature. Steam flows through the tank and the HITEC temperature increases up to its melting point (142 °C) after about 1 h. At this point, isothermal phase change (melting) takes place for about 1 h, after which the PCM becomes a liquid and sensible heat is stored in the tank with a further increase in the liquid PCM temperature.

Similar temporal responses have been obtained for all thermal tanks, which suggests that the tanks are capable of continuously charging and/or discharging over up to 1 h, thereby allowing the EMS concept presented in Fig. 3, during low and peak demand periods. Therefore, we only consider the case when using the PCM for latent heat storage, during which time it remains at its phase change temperature. In practice, charging and discharging rates will be different from those evaluated here due to material non-uniformity and unsteady heat transfer effects, however, the rates for charging should remain within 10–20% of these estimates for charging and the double for discharging [51].

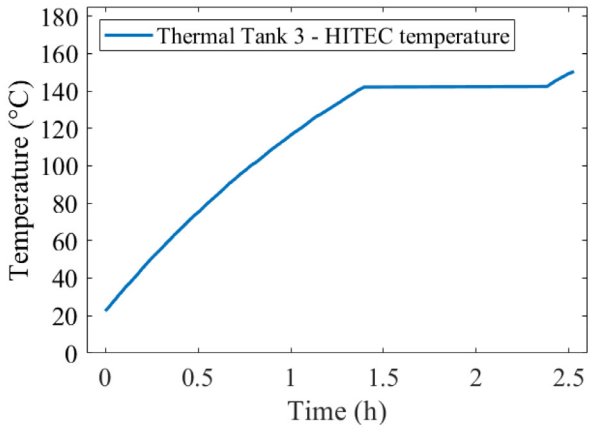

Fig. 12. PCM (HITEC) temperature in Thermal Tank 3 during charging. In this paper, we only consider operation with phase change, in the (isothermal) latent heat storage regime.

4. Results for the EDF nuclear power plant case study

4.1. Plant derating during TES charging

Fig. 13a shows the fractional plant derating during TES charging versus the degree of steam extraction when the three TES schemes in Section 3 are applied to the EdF nuclear power plant. The fractional derating value is the ratio of the net generator output from the base plant with steam extraction to that without steam extraction, i.e., with a maximum net generator output of 670 MW_{el} from the base power plant. From left-to-right the schemes include: (i) 12% steam extraction before the reheater (for details, see Section 3.1); (ii) 80% steam extraction before the LPT (for details, see Section 3.2); and (iii) 12% steam extraction before the reheater and 80% extraction of the remaining steam before the LPT (for details, see Section 3.3). As a result of these three steam extraction strategies, the electrical power output of the power plant decreases and the amount of stored thermal energy increases, as shown from left to right in Fig. 13b.

Fig. 13 suggests that it is possible to use existing nuclear power plants (Gen. I and II) for flexible generation in load following with a maximum derating of 40%, with minimum loads down to 60% of a plant's rating. The stored thermal energy increases with the amount of steam extraction up to a total of 822 MW_{el} (see Table 6), as the net power output reduces by 40%, from 670 MW_{el} to a minimum of 406 MW_{el}. It is interesting to note that the greatest flexibility of the power plant, and therefore the largest potential for load following, is attained for low-temperature TES, when extracting steam before the LPT. Furthermore, Fig. 14a shows the heat input (rate) to the plant and Fig. 14b the plant efficiency during TES charging for the same three steam extraction schemes as in Fig. 5. The heat input is maximum when steam is not extracted or when it is extracted only before the LPT when heat is stored at the lowest temperature. When steam is extracted before the reheater the total input to the plant drops by 1.5%. As a result of the steam extraction, the thermal efficiency of this particular nuclear plant reduces from 43% (for full-load plant operation) to 26% (for 60% part-load operation).

4.2. EMS cost assessment

A simple cost analysis is performed on the proposed EMS (i.e., with three thermal tanks and two ORC plants) to determine at what extent it is an economically viable solution. The cost analysis starts by determining the levelised cost of electricity (LCOE) of the proposed thermal tanks and both ORC systems for each discharging cases (A, B, C, and D of Table 4). The LCOE is calculated from:

$$LCOE_{\mathrm{EMS}} = \frac{\sum_{t=1}^{n} \frac{C_1 + O\&M_t + CH_t}{(1+r)^t}}{\sum_{t=1}^{n} \frac{E_t}{(1+r)^t}} \tag{20}$$

where C_1 is the capital cost of the thermal tanks and the ORC systems in year 1, $O\&M_t$ the operation and maintenance expenditure in year t, CH_t the charging cost in year t, E_t the electricity generation from both ORC systems in year t, r the discount rate, and n the life of the system.

The new parameter in the LCOE formula is the charging costs (CH) which accounts for the cost of selling less amount of electricity while charging the thermal tanks. All LCOE calculation parameters are presented in Table 7. The capital costs of the ORC plants are estimated by taking the average of the investment costs of similar-sized ORC plants from the literature [55,62,63].

4.2.1. Electricity prices

In order to evaluate the profitability of the proposed flexible generation system, the wholesale (day-ahead) hourly electricity prices in the UK over the year 2019 are taken as a baseline and a further analysis is performed based on the electricity prices in 2021 (until 15 Nov.) [61]. The calculations are performed assuming that the generated electricity

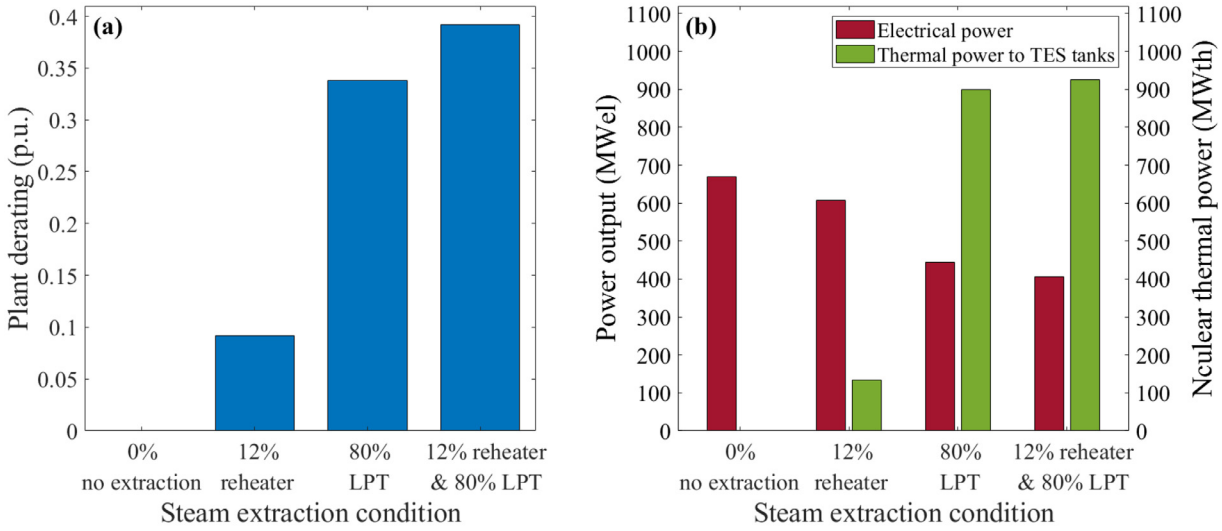

Fig. 13. (a) Fractional plant derating, and (b) power output of main/base nuclear power plant and stored thermal energy during TES charge, for the three EMS schemes proposed herein.

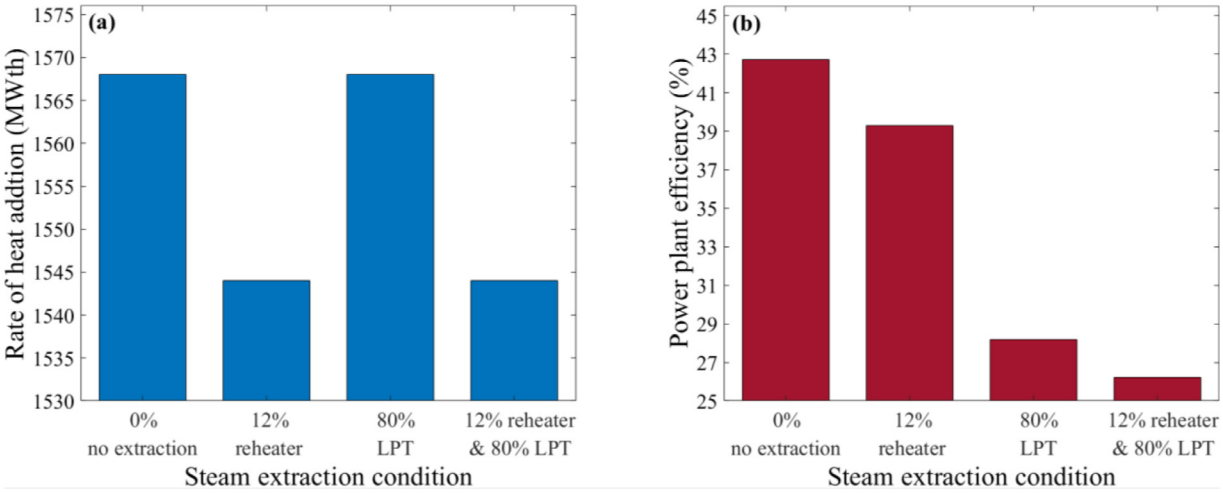

Fig. 14. (a) Heat input (rate), and (b) efficiency of main/base nuclear power plant during TES charge, corresponding to the same three EMS schemes as in Fig. 5.

Table 7
Cost and LCOE calculation parameters [55,62–64].

Cost analysis parameters	Value
ORC systems capital costs (£/kW_{el})	1140
TES system capital costs (£/kWh)	25
Operation & maintenance (%)	3% of capital cost
Charging cost per day (£/day)	264 (MWh) × $\overline{EP}_{1,Ch}$ (£/MWh) for one 1-h charge per day
	528 (MWh) × $\overline{EP}_{2,Ch}$ (£/MWh) for two 1-h charges per day
Project lifetime (years)	25
Discount rate (%)	3
Availability factor (%)	90
Projected annual electricity output (GWh)	49.8 for one 1-h charge per day
	99.6 for two 1-h charges per day

Table 8
Calculated average hourly electricity price for charging and discharging; the average is calculated based on UK electricity market data for years 2019 and 2021 (until 15 Nov.) [61].

Average hourly price (£/MWh)			Definition and number of hourly prices per day	Charging or discharging duration conditions
Parameter	2019	2021		
$\overline{EP}_{1,Ch}$	30.2	65.9	Minimum price per day (1 h)	One 1-h charge
$\overline{EP}_{2,Ch}$	30.7	67.2	Minimum price per day (2 h)	Two 1-h charges
$\overline{EP}_{1,Dch}$	63.0	202	Maximum price per day (1 h)	One 1-h discharge (Case A)
$\overline{EP}_{2,Dch}$	60.6	182	Maximum price per day (2 h)	One 2-h discharge (Case B)
				Two 1-h discharges (Case A)
$\overline{EP}_{4,Dch}$	57.1	159	Maximum price per day (4 h)	One 4-h discharge (Case C)
				Two 2-h discharges (Case B)
$\overline{EP}_{8,Dch}$	52.8	136	Maximum price per day (8 h)	One 8-h discharge (Case D)
				Two 4-h discharges (Case C)
$\overline{EP}_{16,Dch}$	47.7	115	Maximum price per day (16 h)	Two 8-h discharges (Case D)

will be entirely sold in the day-ahead or intraday electricity market. However, the electricity generators may consider the option of selling the generated electricity at different markets such as the balancing market (BM), fast frequency response (FFR), net imbalance volume (NIV) chasing technique, etc., which varies in terms of risk and rewards [65]. Furthermore, it is assumed that the secondary power plants have a rapid ramp rate, meaning that the power plant goes from zero to full-rated power or vice versa within a few minutes, so being able to provide the required services to the grid. This means that the ORC plants should operate as a spinning reserve being able to quickly enter into service, incurring in no-load losses that are not explicitly quantified in this study.

Table 8 summarises the hourly electricity prices $\overline{EP}$ assumed in the economic analysis, and in particular the prices during charging and discharging periods. The second column of Table 8 defines the selection of these prices and the third column summarises the conditions in which these prices are applied in the analysis. As mentioned previously, the prices are yearly averaged and calculated using the minimum or the maximum hourly price during each day:

$$\overline{EP} = \frac{\sum_{i=1}^{365} \left[\min \text{ or } \max\left(EP_1, EP_2, \ldots, EP_{24}\right)\right]}{365} \tag{21}$$

4.2.2. Capacity payment

In addition to the revenues from selling electricity in the wholesale electricity market, power generators are entitled to participate in the UK capacity market. The capacity market is established to ensure security of electricity supply and enhanced capability to match variable demand. This is satisfied by the UK's government providing an incentive (i.e., capacity payment) for power plants that are available to quickly enter into service if needed by the power system during periods of high demand or low unexpected availability of the intermittent renewable sources. The

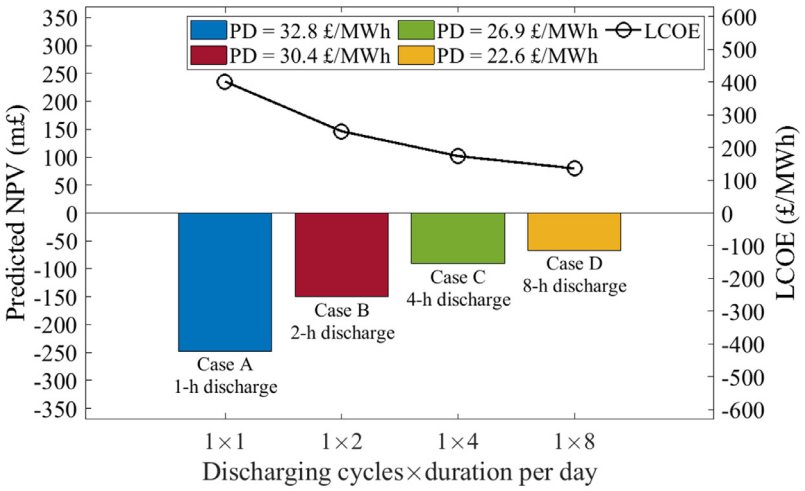

Fig. 15. Predicted NPV, on the left *y*-axis, and calculated LCOE, on the right *y*-axis, of the proposed EMS with three thermal tanks and two ORC systems for all the four cases of discharging duration (i.e., A, B, C, and D) and one discharge per day. The figure presents results assuming UK wholesale electricity prices in year 2019 and one 1-h charge per day at the minimum electricity price.

Table 9
Assumed capacity payment of all discharging cases [67].

Case (duration)	A (1 h)	B (2 h)	C (4 h)	D (8 h)
Derating factor (%)	36.4	64.4	96.1	96.1
ORC systems power (MW_{el})	152	75.8	37.9	19.0
Annual capacity payment (k£)	896	796	591	296

capacity payment encourages new investments in the energy sector as it guarantees a fixed amount of income for generators [66]. In this study, the amount of the capacity payment is assumed as 16.2 £/kW_{el}/year, which is the average of the five years' clearing prices (i.e., from 2015 to 2019) in the four-year ahead delivery capacity auctions [67]. However, energy or electricity storage systems do not get paid the full amount of the clearing price since most of the systems have a limited discharging duration. Therefore, the UK government has provided a derating factor which specifies the payment in percent in the bases of duration, and which penalises plants with a shorter time of operation per day [68]. Table 9 summarises the assumed capacity payment for the proposed discharging cases (i.e., A, B, C, and D). The derating factor reported in Table 9 is multiplied by the average unitary capacity payment to get the total annual capacity payment for each proposed ORC systems size.

4.2.3. Economic analysis based on UK wholesale electricity prices in 2019

The economic evaluation is performed by calculating the projected net present value (NPV) of the proposed EMS investment:

$$NPV_{\mathrm{EMS}} = \sum_{t=1}^{n} \frac{I_t + CP_t}{(1+r)^t} - \sum_{t=1}^{n} \frac{C_1 + O\&M_t + CH_t}{(1+r)^t} \tag{22}$$

where I_t is the annual income from selling extra electricity from ORC generators during peak prices, which depends on the number of discharging hours per day and on the annual capacity payment CP_t.

Fig. 15 presents the estimated net present value, on the left *y*-axis, alongside with the calculated LCOE, on the right *y*-axis, for the different discharging duration times. It also indicates the average electricity price difference (PD) between charging and discharging modes for the different cases.

Case A has the highest LCOE of 401 £/MWh due to the highest cost of ORC plants (maximum installed size). The LCOE drops to about 136 £/MWh for Case D as a result of the smaller size of the ORC systems, which are designed to generate the same amount of electricity but over longer durations (i.e., 8 h). However, the LCOE is still considered high and not yet comparable to the LCOE of other competitive energy sources, either renewables or fossil fuelled power plants. Moreover, the predicted NPVs of the proposed EMS for all discharging cases are negative due to two main reasons. The first is that the average price difference between off-peak and peak PD is quite low in the current UK electricity market. The second reason is the high LCOE which is also influenced by the relatively high average of off-peak electricity price (30.2 £/MWh), i.e., an avoided income when charging the thermal tanks. Therefore, the proposed EMS with one 1-h charge per day is not an economically viable option based on 2019 wholesale electricity prices, even with the proposed smallest size of ORC systems that discharges the same amount of thermal power over 8 h per day.

Results obtained with two charge/discharge cycles per day are presented in Fig. 16, which shows a 43% relative decrease of the LCOE (i.e., from 401 to 228 £/MWh) in Case A for the option of two cycles a day. This drop is a result of doubling the amount of electricity generated during the assumed investment lifetime. In Case D, the LCOE drops to 95 £/MWh for the same reasons. However, the NPV is still negative and unprofitable even for two fully charge/discharge cycles per day. This is due to the lower selling price of electricity when full discharging is performed twice a day for all cases, which is seen in the lower PD reported in Fig. 16, in comparison to the previous case. The predicted NPV is even more negative for two 8-h discharges (16 h in total) in Case D (−77.5 m£) than for a single 8-h discharge (−66.8 m£). It is concluded that the EMS profitability greatly depends on the peak and off-peak price difference, which was not sufficiently high in the UK wholesale electricity market in 2019.

A summary of the main economic analysis results of the four examined cases based on 2019 prices, for both one and two discharges per day, are presented in Table 10. The total investment costs that consist of the ORC engine costs and the costs of all thermal tanks drops significantly from Case A to Case D as the size of the ORC systems decreases. Specifically, the investment cost drops to around 48 m£ if single daily discharging is performed for longer durations (i.e., 8-h discharge).

4.2.4. Economic analysis based on UK wholesale electricity prices in 2021

The same economic analysis used in the sections above is performed here for the most recent electricity prices in 2021. During 2021, the electricity prices were much higher and more volatile than in 2019 due to higher natural gas prices, lower wind levels, outages of nuclear plants, and fire damage to electricity interconnectors. The highest and lowest electricity prices recorded in 2021, respectively, were 2500 £/MWh and −19.4 £/MWh, which can be compared to the corresponding 2019 prices of 277 £/MWh and −2.8 £/MWh [61]. Fig. 17 shows the predicted NPV and the LCOE for the four cases with two charge/discharge cycles per day and based on 2021 prices.

The peak and off-peak electricity price spread (PD) in 2021 was much higher than those in 2019 (see Fig. 16), resulting in improved NPVs, however, the NPVs for all examined cases are still negative. For example,

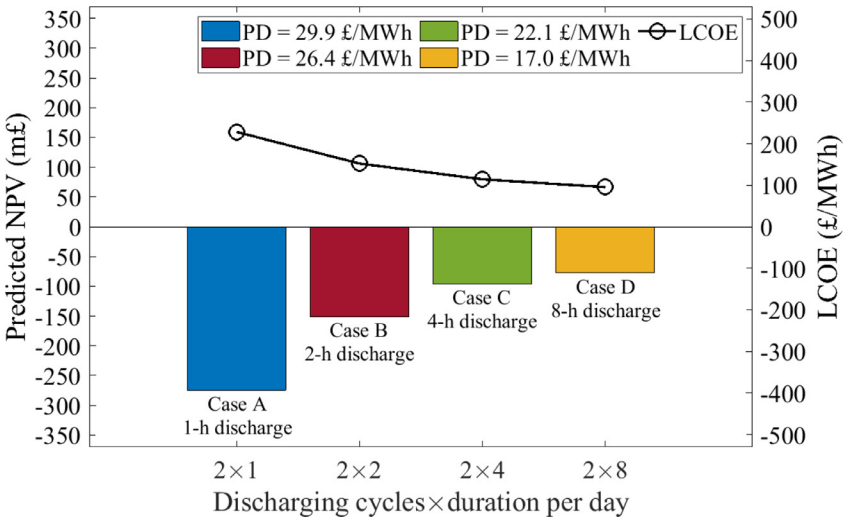

Fig. 16. Predicted NPV, on the left *y*-axis, and calculated LCOE, on the right *y*-axis, of the proposed EMS with three thermal tanks and two ORC systems for all the four cases of discharging duration (i.e., A, B, C, and D) and two discharges per day. The figure presents results assuming UK wholesale electricity prices in year 2019 and two 1-h charges per day at the minimum electricity price.

Table 10
Main economic analysis results of the analysed four cases (UK wholesale electricity prices in 2019).

No. of discharges per day	Case	Total EMS investment costs (m£)	O&M costs (m£/year)	Charging costs (m£/year)	Generated electricity (GWh/year)	Total revenues (m£/year)	LCOE (£/MWh)	NPV (m£)
One discharge	A	199	6.0	2.6	49.8	4.0	401	−248
	B	112	3.4	2.6	49.8	3.8	250	−150
	C	69.0	2.1	2.6	49.8	3.4	174	−90.8
	D	47.5	1.4	2.6	49.8	2.9	136	−66.8
Two discharges	A	199	6.0	5.3	99.6	6.9	228	−276
	B	112	3.4	5.3	99.6	6.6	152	−151
	C	69.0	2.1	5.3	99.6	5.8	114	−96.1
	D	47.5	1.4	5.3	99.6	5.0	95.2	−77.5

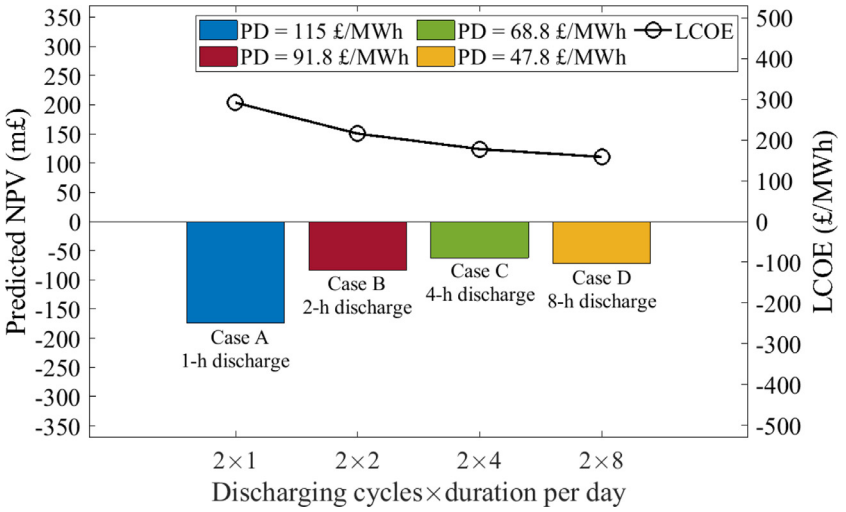

Fig. 17. Predicted NPV, on the left *y*-axis, and calculated LCOE, on the right *y*-axis, of the proposed EMS with three thermal tanks and two ORC systems for all the four cases of discharging duration (i.e., A, B, C, and D) and two discharges per day. The figure presents results assuming UK wholesale electricity prices in year 2021 and two 1-h charges per day at the minimum electricity price.

the NPV for Case A with two charges/discharges per day improves by 37% relative to the one calculated based on 2019 prices. Moreover, the LCOEs calculated based on 2021 prices are higher than those calculated based on 2019 prices because of the higher averaged off-peak (charging) prices in 2021 (i.e., 67.2 £/MWh compared to 30.7 £/MWh in 2019).

Interestingly, it can be seen from Fig. 17 that Case D has a lower NPV than Case C, which was not the case in the obtained results using 2019 prices (i.e., in Figs. 15 and 16). Although Case D has lower EMS investment and O&M costs due to reduced size of the ORC systems, the relative decrease in the total investment costs for Case D relative to Case C is lower than the relative decrease in total revenues gained from selling electricity at a lower average price, which results in a higher NPV for Case C. This implies that the economics of the EMS has several competing factors, including the EMS investment costs and difference between the peak and off-peak prices. The obtained results support the need for finding the optimum size of the ORC systems, optimum duration of the TES charge/discharge cycles, and the optimum frequency of the cycles that yield the highest NPV for given electricity prices. This optimisation exercise is an interesting area of future work.

The best projected LCOE when considering 2021 decreases to 159 £/MWh when doubling the total amount of generated electricity, i.e., 100 GWh/year, by having two 1-h charge and 8-h discharge cycles

Table 11
Considered pricing scenarios for sensitivity analysis of the proposed EMS solutions.

Scenario number	Off-peak price decrease*	Charging prices (£/MWh)		Peak price increase*	Discharging prices (£/MWh)				
		$\overline{EP}_{1,Ch}$	$\overline{EP}_{2,Ch}$		$\overline{EP}_{1,Dch}$	$\overline{EP}_{2,Dch}$	$\overline{EP}_{4,Dch}$	$\overline{EP}_{8,Dch}$	$\overline{EP}_{16,Dch}$
1	10%	27.2	27.7	50%	94.5	90.9	85.6	79.2	71.2
2	25%	22.6	23.1	100%	126	121	114	106	94.9
3	50%	15.1	15.4	150%	158	151	143	117	118
4	75%	7.5	7.7	200%	189	182	171	158	142

* Relative to the prices in 2019 in Table 8, and considered in Sections 4.2.1 to 4.2.3.

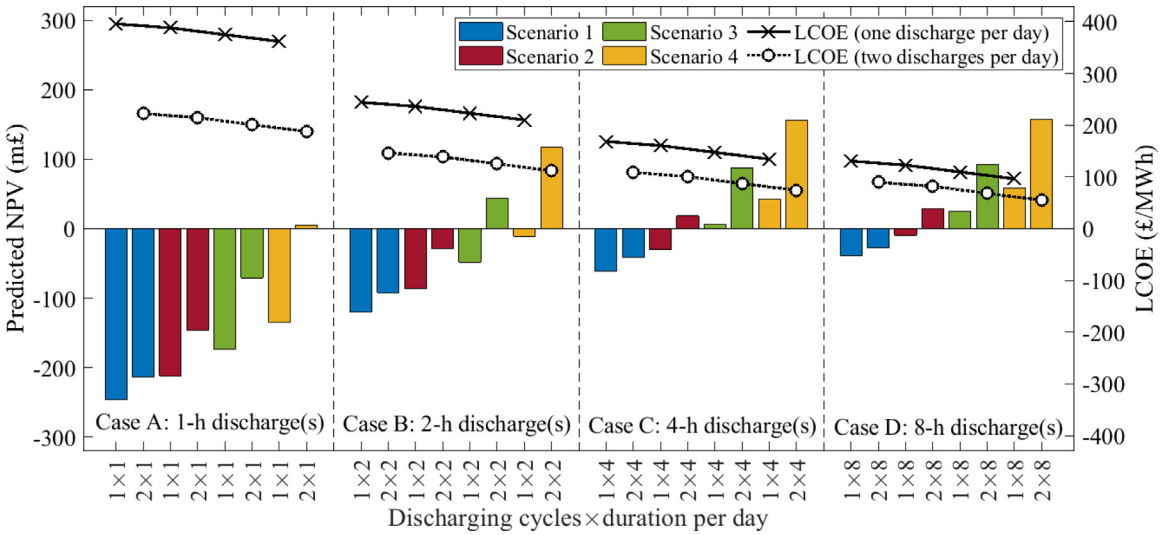

Fig. 18. Predicted NPV, on the left *y*-axis, and calculated LCOE, on the right *y*-axis, of the EMS for the proposed price increase scenarios. The presented results are obtained considering all four discharging duration cases (i.e., Cases A, B, C, and D) and the two charging options (i.e., one 1-h charge and two 1-h charges) per day.

per day (Case D), and the NPV increases to −48.6 £/MWh with one 1-h charge and 8-h discharge cycle per day (Case D).

4.2.5. *Assessment of different electricity price scenarios*

The electricity market is volatile, and prices can rapidly change on an hourly, daily and longer-term basis (e.g., the trend of the UK wholesale electricity market). Therefore, different electricity price scenarios are considered here, to evaluate the potential future profitability of the EMS system. The considered pricing scenarios are summarised in Table 11. These scenarios can also be applied for different electricity markets in the world that have relatively similar capacity payments to the UK's.

Fig. 18 shows the predicted NPV, on the left *y*-axis and the calculated LCOE, on the right *y*-axis, of the EMS at the four proposed electricity price scenarios. The economic evaluation is performed for all discharging cases (i.e., Cases A, B, C, and D), and for both a single charging/discharging cycle and two charging/discharging cycles per day. Therefore, results relating to 32 combinations of discharging cases and price scenarios are summarised in this figure.

The LCOE drops significantly when a complete charging/discharging cycle is performed twice per day, as a result of doubling the amount of electricity generated at peak demand periods. Moreover, the LCOE of each case declines slightly from price Scenario 1 to Scenario 4, due to the lower average charging costs (which are the lowest for Scenario 4). The lowest LCOE corresponds to a discharging of 16 h a day (i.e., two 8-h discharge cycles per day) at price Scenario 4. This relatively low LCOE is achieved as the capital costs of the ORC systems and the charging costs are at their lowest amongst the cases considered here. As can be seen, many the combinations are associated with negative LCOEs even with the increased selling price at peak demand, but 13 combinations provide positive NPV, at longer discharge durations and with two charge/discharge cycles per day. In general, these results suggest that a positive NPV can result when the average peak and off-peak electricity price variations are at least double those that occurred in the UK market in 2019, and with TES charge/discharge cycles are performed more than once per day with a discharge duration to the ORC plants longer than 2 h. Of importance and with important implications for the future, is the fact that recent electricity price data in the UK are now approaching this limit.

Electricity market price variations during the day are key factors for the profitability of the proposed EMS solutions. Therefore, the breakeven discharging prices, at different TES charging prices, to obtain NPV equal to zero, are presented in Fig. 19. The minimum average electricity price for all cases and for four different average off-peak prices (AOP) are compared. In every case, the minimum peak price decreases as the AOP declines from 20 to 5 £/MWh. Moreover, the required minimum peak price reduces significantly as the discharging cycle is performed twice a day, especially in Case A and Case B. Taking Case B with two full charges a day and with an AOP of 5 £/MWh, the EMS could be profitable if the averaged peak prices (for 4 h a day) are above 99.2 £/MWh. In conclusion, the flexible nuclear plant configuration with EMS could be a profitable option in a highly fluctuating electricity market with a large difference between off-peak and peak electricity prices.

5. Conclusions

An energy management system (EMS) for the flexible operation of power plants based on generation-integrated thermal energy storage (TES) has been proposed and applied to an existing 670 MW_{el} Rankine-cycle nuclear power plant operated by EdF as a case study. The options of steam extraction before the reheater and/or before the low-pressure turbine (LPT) of the power plant during off-peak demand have been investigated.

In this EMS, steam is extracted from the power plant during off-peak demand for the charging of the TES, and at a later time when this is

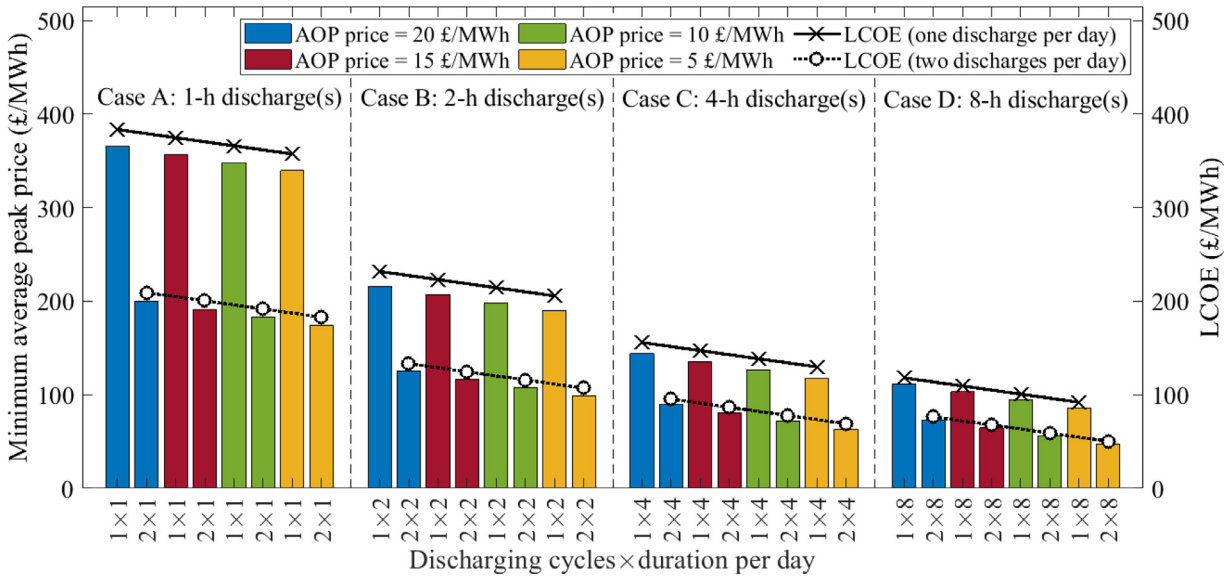

Fig. 19. Minimum average electricity peak price at discharging, on the left *y*-axis, and resulting LCOE, on the right *y*-axis, for different AOP prices to obtain NPV of the investment equal to 0 for the proposed Cases (A to D) and 1 or 2 full TES charging/discharging per day.

economically favourable these tanks act as the heat sources of secondary thermal power, in particular as evaporators of organic Rankine cycle (ORC) systems that are suitable for extra power generation. As discussed in previous studies in the literature, such as in Ref. [28] and Ref. [29], this type of solution offers greater flexibility than TES-only solutions that store thermal energy and then release this back to the base power plant, in that it allows both derating but also an over-generation compared to the base power plant rating.

In such a scheme, the EMS would be required to optimise the derating of such power plants for the charging of the thermal tanks during off-peak demand periods and to control the discharging of the tanks for electricity generation from the secondary plants during the peak-demand periods. It has been found that when charging the PCM-TES tanks during off-peak demand in a proposed scheme with three TES tanks, a maximum plant derating of 40% can be achieved, i.e., down to 406 MW_{el}. At peak demand, when discharging the PCM-TES tanks, the thermodynamic analysis has suggested that a maximum combined power of 822 MW_{el} can be delivered, which includes the 670 MW_{el} generated by the nuclear power plant and an additional 152 MW_{el} from two secondary generation ORC plants. This is 23% higher than the nuclear plant's full-load rating. The options of lower ORC plant sizes with corresponding longer operating time have been also considered, keeping constant the TES capacity and hence the delivered excess electricity from the ORC systems, but with lower investment costs due to smaller size.

The economic profitability of the proposed integrated storage system has been analysed considering UK hourly prices in the wholesale electricity market during the years 2019 and 2021. It was concluded that profitability of the flexible power plant configuration, defined as a positive net present value (NPV) relative to the business as usual (BAU) operation, can be achieved if: (i) the average peak and off-peak electricity price variations are at least double those that occurred in the UK market in 2019; and (ii) TES discharge duration to the ORC plants is longer than 2 h or the TES charge/discharge cycle is performed more than once a day. Moreover, an investment cost for the case of one 1-h charge and one 1-h discharge per day was estimated at 199 m£ with a total generated electricity of 50 GWh per year, and a LCOE of 401 £/MWh was obtained based on 2019 electricity prices. However, the investment cost drops to around 48 m£ if discharging is performed for longer durations (i.e., 8-h discharge), which reduces the size of the ORC systems. Furthermore, the projected LCOE also decreases to 95 £/MWh when doubling the total amount of generated electricity, i.e., 100 GWh/year, by having two charge/discharge cycles per day. When considering the most recent UK electricity prices in 2021 (to-date), single 1-h charge/discharge cycles per day lead to a LCOE of 463 £/MWh, which decreases to 159 £/MWh when doubling the total generated electricity (100 GWh/year) by employing two daily 8-h TES charge/discharge cycles.

Finally, it was demonstrated that the economics of the EMS, especially in terms of the NPV, are determined by a trade-off between longer discharge durations to the ORC plants that minimises their size and cost, and shorter charge/discharge durations that yield the highest difference between off-peak and peak electricity prices. This highlights the need to identify the optimum (TES and ORC) system design and sizing, as well as the optimum duration of the TES charge/discharge cycles, and the optimum frequency of the cycles that yield the highest NPV for given electricity prices.

In future work, we intend to investigate additional EMS strategies for the provision of ancillary services in transmission networks of smart grids. We also intend to consider such strategies for increasing the thermal efficiencies of the secondary power plants during peak demand. The requirements for fast-start operation of generation plants to provide ancillary services to the grid are becoming more and more important, and the trade-offs between costs of fast response operating modes and revenues from ancillary electricity market sales should be carefully investigated, in order to assist investment and management decisions [69]. We aim to investigate in particular fast-start secondary power plants with aggressive hot starts (which can be, reportedly, within 10 min, and down to 10 s when the plants are at temperature). Such improvements can offer significant benefits to utilities in terms of primary and secondary frequency responses, and consequently higher profitability in ancillary markets and value to the overall energy system.

Declaration of Competing Interests

The authors declare that they have no known competing financial interests or personal relationships that could have appeared to influence the work reported in this paper.

Acknowledgements

This work was supported by the UK Engineering and Physical Sciences Research Council (EPSRC) [grant numbers EP/K002228/1,

EP/P004709/1, EP/R045518/1, and EP/S032622/1]. Data supporting this publication can be obtained on request from ceplab@imperial.ac.uk.

Appendix A–Design of thermal tanks

A.1. Thermal Tank 1

For the calculation of the heat exchange area A and tube length L of Thermal Tank 1, the following set of assumptions are made:

1 The vapour density is much lower than the liquid density as the following:

$$\rho_L \ll \rho_V,\ f \approx 1,\ \delta_F \ll d \tag{A.1}$$

where ρ_L and ρ_V are the vapour-phase (steam) and condensate/liquid-phase (water) densities, f the waviness correction factor of the film flow, δ_F the film thickness, and d the heat exchange tube diameter. Here, we use a number of standard type 316 stainless steel tubes with a diameter $d = 102$ mm and a tube thickness $w = 6$ mm.

2 The velocity of the liquid phase is negligible compared to the velocity of the vapour phase, and the shear stress throughout the vapour phase is negligible.

3 The desuperheating length/area is negligible compared to the condensation length/area.

Given a variable distance z along the heat-exchanger tube of total length L (i.e., inlet at $z = 0$ and outlet at $z = L$) inside the tank, we define local dryness (mass) fractions at points: $\dot{x}_1 = 0.99$, $\dot{x}_2 = 0.90$, $\dot{x}_3 = 0.50$, $\dot{x}_4 = 0.1$, $\dot{x}_5 = 0.01$, $\dot{x}_6 = 0.001$, where for example for the local value $\dot{x}_2$:

$$z_2 = 0.1\ L \text{ corresponds to } \dot{x}_2 = 1 - \frac{z_2}{L} = 0.9 \tag{A.2}$$

In this case, the local value of the dryness fraction, e.g., $\dot{x}_2 = 0.90$ here, is linked to the local liquid-phase mass flowrate $\dot{m}_{L,z}$ and vapour-phase mass flowrate $\dot{m}_{V,z}$ through its definition:

$$\dot{x}_2 = \frac{\dot{m}_{V,z_2}}{\left(\dot{m}_{L,z_2} + \dot{m}_{V,z_2}\right)} = \frac{\dot{m}_{V,z_2}}{\dot{m}_{V,z=0}} \tag{A.3}$$

where conservation of mass was used to replace the local mass flowrates with the vapour mass flowrate of the extracted steam before the reheater at the inlet to Thermal Tank 1, $\dot{m}_{V,z=0}$, since the inlet liquid mass flowrate is zero, $\dot{m}_{L,z=0} = 0$.

The local distribution of the vapour and liquid phases in the pipe can be described by the volumetric vapour-phase fraction $\varepsilon = V_V/(V_V + V_L)$, with V_V and V_L the local vapour and liquid volume phase-fractions, which is given as a function of the flow parameter F from the relation:

$$\varepsilon = 1 - \frac{1}{1 + \frac{1}{8.48\ F}} \tag{A.4}$$

where F is given by:

$$F = \frac{\max\{\left(2\ Re_{L,z}\right)^{0.5};\ 0.132\ Re_{L,z}^{0.9}\}}{Re_{V,z}^{0.9}}\ \frac{\mu_L}{\mu_V}\sqrt{\frac{\rho_V}{\rho_L}} \tag{A.5}$$

and where the two Reynolds numbers, one for each fluid phase, are defined as:

$$Re_{L,z} = \frac{\dot{m}_{L,z}}{\pi\ d\ \mu_L} \tag{A.6}$$

$$Re_{V,z} = \frac{\dot{m}_{V,z}}{\pi\ d\ \mu_V} \tag{A.7}$$

with μ_L and μ_V are the liquid and vapour dynamic viscosities, respectively.

The local heat transfer coefficient in the condensate liquid-film flow is described by a dimensionless Nusselt number. In the laminar film-flow region near the pipe inlet, this can be found from the correlation:

$$Nu_{L,z,La} = \frac{\alpha_{L,z}\ \Lambda}{k_L} = 0.693\left(\frac{1 - \frac{\rho_V}{\rho_L}}{Re_{L,z}}\right)^{1/3} \tag{A.8}$$

whereas in the turbulent region after the transition/entrance length, it can be found from the correlation:

$$Nu_{L,z,Tu} = \frac{\alpha_{L,z}\ \Lambda}{k_L} = \frac{0.0283\ Re_{L,z}^{7/24}\ Pr_L^{1/3}}{1 + 9.66\ Re_{L,z}^{-3/8}\ Pr_L^{-1/6}} \tag{A.9}$$

in both cases based on a characteristic (Nusselt film height) length scale of the film flow:

$$\Lambda = \left(\frac{u_L^2}{g}\right)^{1/3} \tag{A.10}$$

Based on the above, a total Nusselt number $Nu_{L,z}$ can be evaluated:

$$Nu_{L,z} = \sqrt{Nu_{L,z,La}^2 + Nu_{L,z,Tu}^2} \tag{A.11}$$

The local heat transfer coefficient $\alpha_{L,z}$ is defined as:

$$\alpha_{L,z} = \frac{q'_z}{\left(T_{Ph} - T_{w,z}\right)} \tag{A.12}$$

with q'_z the local heat flux on the vertical tube wall, T_{Ph} the temperature at the film free-surface and $T_{w,z}$ the tube wall temperatures, which from the above is given by:

$$\alpha_{L,z} = \frac{K\ Nu_{L,z}\ k_L}{\Lambda} \tag{A.13}$$

that uses a correction factor for shear stress:

$$K = \left(\frac{\tau_V}{\rho_L\ g\ \delta_L}\right)^{1/3} \tag{A.14}$$

where g is gravitational acceleration, and ρ_L and k_L the density and thermal conductivity of water.

The overall heat transfer coefficient U at the local point z_2 is:

$$\frac{1}{U_{z_2}} = \frac{1}{\alpha_{L,z}} + \frac{w}{k} \tag{A.15}$$

where k is the thermal conductivity of 316 stainless steel. It is worth noting that the outer surface temperature of the 316 stainless steel tube is assumed to be equal to the PCM melting temperature of 250 °C. Furthermore, the overall heat transfer coefficient between the two local points is:

$$\bar{U}_{z_{1,2}} = \frac{U_{z_1} + U_{z_2}}{2} \tag{A.16}$$

The necessary tube length between these two local points is given by:

$$\Delta L_{1,2} = \frac{\Delta m_{L,z_{1,2}}\ \Delta h_v}{\pi\ d\ \bar{U}_{z_{1,2}}\ \Delta T} \tag{A.17}$$

Beyond the transfer of latent heat from the condensing steam, sensible heat is also transferred in a section of the tank. For the calculation of the heat transfer in this section, instead of the phase-change enthalpy, the total difference of the specific enthalpies of steam and saturated water is used:

$$\Delta h = \Delta h_v + c_{pV}\left(T_V - T_{sat}\right) = \Delta h_v + c_{pV}\ \Delta T_{Ü} \tag{A.18}$$

The condensation area required is:

$$A_{Ü} = A\left(1 + \frac{c_{pV}\ \Delta T_{Ü}}{\Delta h_v}\right) \tag{A.19}$$

where c_{pV} is the specific heat capacity of the steam and $\Delta T_{Ü}$ the superheated temperature difference. Full details and a procedure from solving these equations are given in Ref. [46].

Since we have evaluated the heat exchange area A and the tube length L, we have to check these values against the pressure drop and the number of tubes in the condenser. These calculations are based on an iterative method by setting arbitrarily the number and the length of the tubes until the pressure drop gives satisfactorily results.

For the calculation of the pressure drop, the shear stress τ_V is given by:

$$\tau_V = \frac{\xi_r}{8}\ \rho_V\ u_V^2 \tag{A.20}$$

where ξ_r is a friction factor for rough pipes that can be found from:

$$\xi_r = \xi_g(1 + 850\ F) \tag{A.21}$$

and ξ_g is the friction factor for smooth pipes that can be evaluated from the correlation:

$$\xi_g = 0.184\ Re_{V,z}^{-0.2} \tag{A.22}$$

Furthermore, the velocity u_V is given by:

$$u_V = \frac{4\ \dot{m}_{V,z}}{\rho_V\ \pi\ \left(d - 2\ \delta_F\right)^2} \tag{A.23}$$

where the film thickness δ_F is found from:

$$\delta_F = \frac{1-\varepsilon}{4}\ d \tag{A.24}$$

for $\varepsilon \geq 0.67$.

The pressure drop between these two points is:

$$\Delta P_{1,2} = \frac{\tau_{V_1} + \tau_{V_2}}{2}\ \frac{4\ \Delta L}{d - \left(\delta_{F_1} + \delta_{F_1}\right)} \tag{A.25}$$

Therefore, the total length of the tubes is given by:

$$\Delta L = \Delta L_{0,1} + \Delta L_{1,2} + \Delta L_{2,3} + \Delta L_{3,4} + \Delta L_{4,5} + \Delta L_{5,6} \tag{A.26}$$

The heat exchange surface area is:

$$A_s = \pi\ d\ \Delta L \tag{A.27}$$

and the total pressure drop is:

$$\Delta P = \Delta P_{0,1} + \Delta P_{1,2} + \Delta P_{2,3} + \Delta P_{3,4} + \Delta P_{4,5} + \Delta P_{5,6} \tag{A.28}$$

Seeking a solution with a pressure drop less than 100 Pa, an acceptable solution is found with a tube length of 120 m and a pressure drop of 67 Pa.

Finally, the required volume of PCM in Thermal Tank 1 for heat transfer to the tank over 1 h, which amounts to a thermal energy storage capacity of 107 MWh, is found from:

$$Q_{TT-1} = \rho_{PCM}\ V_{TT-1}\ \Delta h_{PCM} = \frac{\pi\ D_{TT-1}^2\ L}{4}\ \rho_{PCM}\ h_{PCM} \tag{A.29}$$

where ρ_{PCM} is the density of the PCM, h_{PCM} the phase-change enthalpy of the PCM, Q_{TT-1} the heat storage of 107 MWh, V_{TT-1} the required volume and D_{TT-1} the diameter of the PCM in the tank. The total volume of Thermal Tank 1 is the sum of the volume of the tubes in the tank plus the volume of the PCM in this store and is given by:

$$V_{TT-1} = \frac{\pi}{4}\ D_{TT-1}^2\ L + \frac{\pi}{4}\ d_{o,TT-1}^2\ L \tag{A.30}$$

where $d_{o,TT-1}$ is the outer diameter of the 316 stainless steel tubes, which is 114 mm.

A.2. Thermal Tank 2

The calculation of the dimensionless numbers in the heat transfer equations requires knowledge of the properties of water. These, however, are temperature dependent and therefore the problem of the design of this thermal tank is solved by iteration. The steps of this procedure are as follows:

1 Calculation of the Reynolds number Re:

$$Re = \frac{u_L\ d_i}{\nu_L} \tag{A.31}$$

where u_L is the bulk water velocity in the tubes, d_i the internal diameter of the tubes, and ν_L the kinematic viscosity of water. In our design, we have used 316 stainless steel tubes with an internal diameter of 76 mm and a wall thickness of 1 mm. We have also assumed that the flow in the pipes of Thermal Tank 2 is such that the flow is turbulent.

2 Calculation of the mean Nusselt number $\overline{Nu}$ from the Gnielinski correlation for heat transfer in turbulent flows through tubes:

$$\overline{Nu} = \frac{(\xi/8)\ Re\ Pr}{1 + 12.7\ \sqrt{\xi/8}\ \left(Pr^{2/3} - 1\right)}\left[1 + \left(\frac{d_i}{L}\right)^{2/3}\right] \tag{A.32}$$

where Pr is the Prantdl number and:

$$\xi = (1.8 \log Re - 1.5)^{-2} \tag{A.33}$$

within the following ranges of validity:

$$10^4 \leq Re \leq 10^6, 0.1 \leq Pr \leq 1000, \frac{d_i}{L} \leq 1 \tag{A.34}$$

3 Calculation of the average convective heat transfer coefficient $\bar{\alpha}$ over a length of a tube based on the mean Nusselt number $\overline{Nu}$ from Equation (A.32):

$$\overline{Nu} = \frac{\bar{\alpha}\ d_i}{k_L} \tag{A.35}$$

where k_L is the thermal conductivity of the water.

4 Calculation of the total heat transfer rate to the thermal tank/heat exchanger Q_{TT-2}:

$$Q_{TT-2} = \bar{\alpha}\ n\ A_s\ \Delta T_{LM} = 2\ n\ \pi\ d_i\ L\ \bar{\alpha}\ \Delta T_{LM} \tag{A.36}$$

where n is the number of the tubes, A_s the heat-transfer area of a single tube, and ΔT_{LM} is the logarithmic mean temperature difference which is defined as:

$$\Delta T_{LM} = \frac{\left(T_w - T_{in}\right) - \left(T_w - T_{out}\right)}{\ln\left(\frac{T_w - T_{in}}{T_w - T_{out}}\right)} \tag{A.37}$$

where T_{in} and T_{out} are the inlet and outlet temperatures of the saturated (inlet) and subcooled (outlet) water respectively, and T_w the tube surface temperature which is assumed to be uniform and equal to the PCM melting temperature at 142 °C.

5 Calculation of the pressure drop associated with fully developed flow in each tube [43]:

$$\Delta P = \xi\ \frac{\rho_L\ u_L^2}{2\ d_i}\ L \tag{A.38}$$

where ρ_L is the density of the liquid water, and ξ the friction factor that is obtained from:

$$\xi = (0.790\ \ln Re - 1.64)^{-2} \tag{A.39}$$

valid in the range:

$$3 \times 10^3 \leq Re \leq 5 \times 10^6 \tag{A.40}$$

6 Calculation of the feed pump power associated with this pressure drop:

$$\dot{W} = \frac{n\ \Delta P\ \dot{m}}{\rho_L} \tag{A.41}$$

where $\dot{m}$ is the mass flowrate of water in a single tube.

7 Calculation of physical properties of water at the mean temperature $\bar{T} = T_{in} + T_{out}/2$. The iteration above is repeated by increasing or decreasing the length of the tubes L and number of tubes n until the calculated heat transfer to the tank is almost equal to 26 MW_{th}.

8 Calculation of the required volume of PCM for storing 26 MW_{th} in Thermal Tank 2 over 1 h leads to a thermal energy storage capacity of 26 MWh, is performed using:

$$Q_{TT-2} = \rho_{PCM}\, V_{TT-2}\, h_{PCM} = \frac{\pi\, D_{TT-2}^2\, L}{4}\, \rho_{PCM}\, h_{PCM} \quad (A.42)$$

where Q_{TT-2} the thermal energy storage capacity of Thermal Tank 2, i.e., 26 MWh, ρ_{PCM} the density of the PCM, V_{TT-2} the required volume of the PCM in tank, h_{PCM} the phase-change enthalpy of the PCM, and D_{TT-2} the diameter of the tank.

9 Finally, the total volume of the thermal tank is the sum of the volume of the tubes in the thermal tank plus the volume of the PCM and is given by:

$$V_{TT-2} = \frac{\pi}{4}\, D_{TT-2}^2\, L + \frac{\pi}{4}\, d_{o,TT-2}^2\, L \quad (A.43)$$

References

[1] World Energy Council, Variable renewables integration in electricity systems: how to get it right, world energy perspectives, Renew. Integr. (2016).
[2] D. Pudjianto, C. Ramsay, G. Strbac, Virtual power plant and system integration of distributed energy resources, IET Renew. Power Gener. 1 (1) (2007) 10–16.
[3] P. Lombardi, Z.A. Styczynski, B.M. Buchholz, Optimal Operation of a Distribution Power System With Renewable Generators and Desalination Plants, GCC Power, 2008.
[4] G. Spaguolo, G. Petrone, S.V. Araujo, C. Cecati, et al., Renewable energy operation and conversion schemes: a summary of discussions during the seminar on renewable energy systems, IEEE Ind. Electron. Mag. 4 (1) (2010) 38–51.
[5] N. Gargov, J. Sun, Technical guidance and testing procedure for static and dynamic demand response and battery storage providers of frequency balancing services, national Grid, 2015. Available at: https://www.nationalgrideso.com/document/92406/download [accessed 15.08.2021].
[6] B. Lu, M. Shahidehpour, Short-term scheduling of combined cycle units, IEEE Trans. Power Syst. 19 (3) (2004) 1616–1625.
[7] R. Kehlhofer, B. Rukes, F. Hannenmann, F. Stirnimann, Combined-cycle Gas & Steam Turbine Power Plants, 3rd Edition, PennWell Books, 2009.
[8] T.K. Ibrahim, M.M. Rahman, A.N. Abdalla, Optimum gas turbine configuration for improving the performance of combined cycle power plant, Proc. Eng. 15 (2011) 4216–4223.
[9] C.N. Markides, Low-concentration solar-power systems based on organic Rankine cycles for distributed-scale applications: overview and further developments, Front. Energy Res. 3 (2015).
[10] O.A. Oyewunmi, A.I. Taleb, A.J. Haslam, C.N. Markides, An assessment of working-fluid mixtures using SAFT-VR Mie for use in organic Rankine cycle systems for waste-heat recovery, Comput. Therm. Sci. 6 (4) (2014) 301–316.
[11] O.A. Oyewunmi, A.I. Taleb, A.J. Haslam, C.N. Markides, On the use of SAFT-VR Mie for assessing large-glide fluorocarbon working-fluid mixtures in organic Rankine cycles, Appl. Energy 163 (2016) 263–282.
[12] O.A. Oyewunmi, C.N. Markides, Thermo-economic and heat transfer optimization of working-fluid mixtures in a low-temperature organic Rankine cycle system, Energies 9 (6) (2016) 448.
[13] A.M. Pantaleo, S.M. Camporeale, A. Sorrentino, A. Miliozzi, et al., Hybrid solar-biomass combined Brayton/organic Rankine-cycle plants integrated with thermal storage: techno-economic feasibility in selected Mediterranean areas, Renew. Energy 147 (3) (2020) 2913–2931.
[14] K.M. Powell, T.F. Edgar, Modelling and control of a solar thermal power plant with thermal energy storage, Chem. Eng. Sci. 71 (2012) 138–145.
[15] S. Kuravi, J. Trahan, D.Y. Goswami, M.M. Rahman, E.K. Stefanakos, Thermal energy storage technologies and systems for concentrating solar power plants, Prog. Energy Combust. Sci. 39 (4) (2013) 285–319.
[16] F. Alobaid, N. Mertens, R. Starkloff, T. Lanz, et al., Progress in dynamic simulation of thermal power plants, Prog. Energy Combust. Sci. 59 (2017) 79–162.
[17] K. Roth, V. Scherer, K. Behnke, Enhancing the dynamic performance of electricity production in steam power plants by the integration of transient waste heat sources into the feed-water pre-heating system, Int. J. Energy Technol. Policy 3 (1/2) (2005) 50–65.
[18] W. Zehtner, H. Spliethoff, W. Woyke, Analysis and optimization of operation of modern hard coal-fired power plants through simulation, VGB PowerTech 88 (11) (2009) 28–32.
[19] R. Starkloff, F. Alibaid, K. Karner, B. Epple, et al., Development and validation of a dynamic simulation model for a large coal-fired power plant, Appl. Therm. Eng. 91 (2015) 496–506.
[20] M. Richter, F. Starinski, A. Starinski, G. Oeljeklaus, K. Gorner, Flexibilization of coal–fired power plants by dynamic simulation, in: Proceedings of the 11th International Modelica Conference, Versailles, France, 2015.
[21] L. Pouret, W.J. Nuttal, Can nuclear power be flexible?, Working Papers EPRG 0710, Energy Policy Research Group, Cambridge Judge Business School, University of Cambridge, 2007.
[22] Nuclear Energy Agency (NEA)Technical and Economic Aspects of Load Following With Nuclear Power Plants, Organisation for Economic Co-operation and Development (OCED), 2011.
[23] International Atomic Energy Agency (IAEA), Non-baseload operations in nuclear power plants: load following and frequency control flexible operations, IAEA Nuclear Energy Series No. NP-T-3.23, Vienna, 2014.
[24] J. Persson, K. Andgren, M. Engström, A. Holm, et al., Lastfoljning I Karnkraftverk: möjliga effektregleringar för svenska kärnkraftverk utifrån ett internationellt perspektiv, 12 Elforsk, 2011.
[25] H. Ludwig, T. Salnikova, A. Stockman, U. Waas, Load cycling capabilities of German nuclear power plants (NPP), VGB PowerTech 91 (38) (2011).
[26] A.A. Al Kindi, A.M. Pantaleo, K. Wang, C.N. Markides, Optimal system configuration and operational strategies of flexible hybrid nuclear-solar power plants, The 33rd International Conference on Efficiency, Cost, Optimisation, Simulation and Environmental Impact of Energy Systems, 2020.
[27] F. Carlson, J.H. Davidson, N. Tran, A. Stein, Model of the impact of use of thermal energy storage on operation of a nuclear power plant Rankine cycle, Energy Convers. Manag. 181 (2019) 36–47.
[28] F. Carlson, J.H. Davidson, On the use of thermal energy storage for flexible baseload power plants: thermodynamic analysis of options for a nuclear Rankine cycle, J. Heat Transf. 142 (2020) article no: 052904.
[29] F. Carlson, J.H. Davidson, Parametric study of thermodynamic and cost performance of thermal energy storage coupled with nuclear power, Energy Convers. Manag. 236 (2021) article no: 114054.
[30] P. Denholm, J.C. King, C.F. Kutcher, P.P.H. Wilson, Decarbonizing the electric sector: combining renewable and nuclear energy using thermal storage, Energy Policy 44 (2012) 301–311 2012.
[31] C.W. Forsberg, Variable and assured peak electricity production from base-load light-water reactors with heat storage and auxiliary combustible fuels, Nucl. Technol. 205 (3) (2019) 377–396.
[32] K. Borowiec, A. Wysocki, S. Shaner, M.S. Greenwood, M. Ellis, Increasing revenue of nuclear power plants with thermal storage, J. Energy Res. Technol. 142 (2020) article no: 042006.
[33] C.W. Forsberg, Hybrid systems to address seasonal mismatches between electricity production and demand in nuclear renewable electrical grids, Energy Policy 62 (2013) 333–341.
[34] C. Forsberg, D.C. Stack, D. Curtis, N.A. Sepulveda, Converting excess low-price electricity into high-temperature stored heat for industry and high-value electricity production, Electricity J. 30 (2017) 42–52.
[35] C. Forsberg, S. Brick, G. Haratyk, Coupling heat storage to nuclear reactors for variable electricity output with baseload reactor operation, Electricity J. 31 (2018) 23–31.
[36] C.W. Forsberg, Heat in a bottle, Mech. Eng. 141 (2019) 36–41.
[37] Y. Li, H. Cao, S. Wang, Y. Jin, et al., Load shifting of nuclear power plants using cryogenic energy storage technology, Appl. Energy 113 (2014) 1710–1716.
[38] M. Green, P. Sabharwall, M.G. Mckellar, S. Yoon, et al., Nuclear Hybrid Energy system: Molten Salt Energy Storage, Idaho National Laboratory, 2013 report no. INL/EXT-13-31768.
[39] K.F. Amuda, R.M. Field, nuclear heat storage and recovery for the APR1400, J. Energy Storage 28 (2020) article no: 101171.
[40] A. Kluba, R. Field, Optimisation and exergy analysis of nuclear heat storage and recovery, Energies 12 (2019) article no: 4205.
[41] M.J. Moran, H.N. Shapiro, Vapor power systems, in: Fundamentals of Engineering Thermodynamics, 4th Edition, John Wiley & Sons, USA, 1999, pp. 372–414.
[42] Central Electricity Generating Board (CEGB), Feed water, in: Heating systems, Modern Power Station Practice„ 2nd Edition, Pergamon Press, Oxford, UK, 1971, pp. 131–213.
[43] J.J. Carberry, Media for heat transport, Chem. Eng. 60 (6) (1953) 225–228.
[44] D. Kearney, U. Herrmann, P. Nava, B. Kelly, et al., Assessment of a molten salt heat transfer fluid in a parabolic trough solar field, J. Sol. Energy Eng. 152 (2) (2003) 170–176.
[45] J.D. McTigue, A.J. White, C.N. Markides, Parametric studies and optimization of pumped thermal electricity storage, Appl. Energy 137 (2015) 800–811.
[46] D.M. Crandall, E.F. Thacher, Segmented thermal storage, Sol. Energy 77 (4) (2004) 435–440.
[47] I. Sarbu, A. Dorca, Review on heat transfer analysis in thermal energy storage using latent heat storage systems and phase change materials, Int. J. Energy Res. 43 (2019) 29–64.
[48] J. Freeman, K. Hellgardt, C.N. Markides, An assessment of solar-powered organic Rankine cycle systems for combined heating and power in UK domestic applications, Appl. Energy 138 (2015) 605–620.
[49] HITEC® Heat Transfer Salt, Coastal Chemical Co., L.L.C, Brenntag Company, Houston, Texas, United States. Available at: http://stoppingclimatechange.com/MSR%20-%20HITEC%20Heat%20Transfer%20Salt.pdf [accessed 10.11.2020].
[50] N. Boerema, G. Morrison, R. Taylor, G. Rosengarten, Liquid sodium versus Hitec as a heat transfer fluid in solar thermal central receiver systems, Sol. Energy 14 (2012) 2293–2305.
[51] A. Gupta, R. Mathie, C.N. Markides, An experimental and computational investigation of a thermal storage system based on a phase change material: heat transfer and performance characterization, Comput. Therm. Sci. 6 (4) (2014) 341–359.
[52] Z. Elmaazouzi, M. El Alami, H. Agalit, E.G. Bennouna, Performance evaluation of latent heat TES system-case study: dimensions improvements of annular fins exchanger, Energy Repor. 6 (2020) 294–301.
[53] X. Zhang, L. Wu, X. Wang, G. Ju, Comparative study of waste heat steam SRC, ORC and S-ORC power generation systems in medium-low temperature, Appl. Therm. Eng. 106 (2016) 1427–1439.
[54] E.W. Lemmon, I.H. Bell, M.L. Huber, M.O. McLinden, NIST Standard reference database 23: reference fluid thermodynamic and transport properties-REFPROP, Version 9.0, 2018.

[55] J. Song, P. Loo, J. Teo, C.N. Markides, Thermo-economic optimization of organic Rankine cycle (ORC) systems for geothermal power generation: a comparative study of system configurations, Front. Energy Res. 8 (6) (2020).
[56] J. Song, C. Gu, Analysis of ORC (organic Rankine cycle) systems with pure hydrocarbons and mixtures of hydrocarbon and retardant for engine waste heat recovery, Appl. Therm. Eng. 89 (2015) 693–702.
[57] D. Matuszewska, P. Olczak, Evaluation of using gas turbine to increase efficiency of the organic Rankine cycle (ORC), Energies 13 (13) (2020).
[58] S. Eyerer, F. Dawo, J. Kaindl, C. Wieland, H. Spliethoff, Experimental investigation of modern ORC working fluids R1224yd(Z) and R1233zd(E) as replacements for R245fa, Appl. Energy 240 (2019) 946–963.
[59] J. Bao, L. Zhao, A review of working fluid and expander selections for organic Rankine cycle, Renew. Sustain. Energy Rev. 24 (2013) 325–342.
[60] J. Zhu, H. Bo, T. Li, K. Hu, K. Liu, A thermodynamics comparison of subcritical and transcritical organic Rankine cycle system for power generation, J. Cent. South Univ. 22 (2015) 3641–3649.
[61] NORD POOL, Historical market data. Available at: www.nordpoolgroup.com/historical-market-data [accessed 20.11.2021].
[62] S. Lemmens, A perspective on costs and cost estimation techniques for organic Rankine cycle systems, 3rd International Seminar on ORC Power Systems, 2015.
[63] S. Quoilin, M. Van Den Broek, S. Declaye, P. Dewallef, V. Lemort, Techno-economic survey of organic Rankine cycle (ORC) systems, Renew. Sustain. Energy Rev. 22 (2013) 168–186.
[64] I. Sarbu, C. Sebarchievici, A comprehensive review of thermal energy storage, Sustainability 10 (191) (2018).
[65] P. Panagiotakopoulou, Different types of electricity markets modelled using PLEXOS integrated energy model- the UK balancing market example, energy exemplar. Available at: https://energyexemplar.com/wp-content/uploads/Different-types-of-electricity-markets-modelled-using-PLEXOS-Integrated-Energy-Model-_The-UK-Balancing-Market-example.pdf [accessed 25.6.2020].
[66] ENGIE, Understanding the capacity market, Leeds, UK. Available at: www.engie.co.uk/wp-content/uploads/2016/07/capacitymarketguide.pdf [accessed 19.8.2021].
[67] National Grid ESO, Electricity Market Reform – Delivery body, Auction results. Available at: https://www.emrdeliverybody.com/CM/Capacity%20Auction%20Information.aspx [accessed 25.6.2020].
[68] Department for Business, Energy & Industrial StrategyCapacity Market Consultation – Improving the framework, Government Response, Crown, London, UK, 2017.
[69] M. Eddington, M. Osmundsen, I. Jaswal, J. Rowell, B. Reinhart, Fast start combined cycles: how fast is fast?, Power Eng., 2017. Available at: www.power-eng.com/articles/print/volume-121/issue-3/features/fast-start-combined-cycles-how-fast-is-fast.html [accessed 25.6.2020].

Panagiotis Romanos

Dr. Panagiotis Romanos graduated with a PhD in Energy Engineering from Kassel University, Germany, in 2007. He is currently the Director of Romanos Engineering Consultancy Ltd. in the UK. He specialises in microgrids, dispersed and RES generation, applied thermodynamics, heat transfer processes as applied to demand side management strategies and high energy efficient conversion and/or storage technologies. He is a member of the Technical Chamber of Greece and Chartered Engineer of the Institution of Engineering and Technology (IET) in the UK.

Abdullah A. Al Kindi

Abdullah Al Kindi is a PhD student in the Clean Energy Processes (CEP) Laboratory of the Department of Chemical Engineering at Imperial College London, working under the supervision of Professor Christos N. Markides. His PhD research focuses on designing, analysing, and optimising a hybrid nuclear-solar power stations with integrated thermal energy storage. He graduated with an MPhil degree in Nuclear Energy from the University of Cambridge, UK. He also holds two BSc degrees in Nuclear and Civil Engineering from the Pennsylvania State University, USA.

Antonio M. Pantaleo

Professor Antonio M. Pantaleo is a part-time Research Fellow in the Clean Energy Processes (CEP) Laboratory of the Department of Chemical Engineering of Imperial College London and Associate Professor of Energy Systems at the University of Bari, Italy. He specializes in thermo-economic modelling of energy-conversion systems, energy systems engineering, supply chains modelling and optimization and bioenergy routes and energy inputs in agriculture. His current research includes the development of energy-system modelling methods that help entrepreneurs to take investment decisions and engineers to identify energy savings and efficiency improvements in processes and energy-conversion systems. These methods combine thermodynamic analysis, process modelling, process integration and optimization techniques and are validated on real scale cases from the industry. He holds an MSc degree in Electrical Engineering, a PhD in Energy Engineering and has 20 years of experience in energy systems modelling as lecturer and research associate/fellow.

Christos N. Markides

Professor Christos N. Markides graduated with a PhD in Energy Engineering from the University of Cambridge, UK, in 2005. He is currently a Professor of Clean Energy Technologies and Head of the Clean Energy Processes (CEP) Laboratory at Imperial College London. He specializes in applied thermodynamics, fluid flow and heat/mass transfer processes as applied to high-performance devices, technologies and systems for thermal-energy recovery, utilization, conversion and/or storage. He is, amongst other, the Editor-in-Chief of Applied Thermal Engineering, a Senior Editor of e-Prime, and an acting member of the UK National Heat Transfer Committee and the UK Energy Storage SUPERGEN Hub.